# Brain Tumor Segmentation by Generative Adversarial Network (GAN)

By

**Jale Guluzade**

Master Thesis

Submitted in Fulfillment of the Requirement

For the Degree of Master of Science

Supervisor:
PhD. Amir Masoud Rahmani

Advisor:

PhD. Behnam Kiani Kalejahi

Khazar University

School of Science and Engineering

2021

Baku, Azerbaijan

## Acknowledgements

This document is written in the spring 2021 as a master thesis to fulfill the requirement for degree of Master of Science. Due to my specialization in Computer Engineering at Khazar University and my related courses, I chose Brain Tumor Segmentation by Generative Adversarial Networks (GAN) for my final thesis as this topic clearly follows my practical and analytical knowledge on this field.

In this thesis, I tried to apply my general knowledge and ability for both practical and technical aspects of GAN through a multiple segmentation methods. I provided a couple of relative images to better explain results of the segmentation algorithms. For that reason, I worked on several articles and data to review literatures based on Magnetic Resonance Imaging (MRI), evolution of Generative Adversarial Networks (GAN) technology, and competitiveness of future segmentation technology for brain tumor segmentation. The readers will gain a basic knowledge and general guidance about medical technology representing realistic images for segmentation in order to become closer to an initiative of future GAN based technologies.

I would like to express my sincere gratitude towards management of Khazar University, professors, instructors and their assistants supporting us to experience on these fields during our master program. Many thanks to my advisor Phd. Behnam Kiani Kalejahi for his valuable and supportive guidance who helped me to research in all aspects of this topic.

## Abstract

The concept of a brain tumor is one of the most significant health issues in terms of both economic and social stability. This disease is extensive growth of abnormal cells in the brain and any growth inside can lead to any serious problem. The cost of a patient's life is a primary concern, so multiple monitoring and treatment systems are still improving to build up the long-term life expectancy of the better life of those patients who have severe brain tumor problems. However, there exists a lack of data available associated with medical diagnosis and images in which intensive diagnostic analytics (DA) techniques are demanded today. In these cases, accurate performance improvement is a major factor of positive enhancement in treatment and diagnostics by the fact that a lack of medical images has constant distribution compared with real image distributions. Therefore, deep learning of structural variability of brain tumors substantially offers contrast-enhanced images to eliminate attainable data gaps and lacks in image distribution.

### Keywords

Brain tumors, Segmentation methods, Magnetic Resonance Imaging (MRI) images, Generative Adversarial Networks (GAN), Low-grade gliomas (LGG), High-grade gliomas (HGG), Image resolutions.

# Table of Contents

# CHAPTER 1

## Introduction

Statistically, incidence rate of brain tumors for women is 26.55 per 100,000 and this rate for men is 22.37 per 100,000 on average. The most dangerous occurring type of these tumors are known as Gliomas. The form of cancerous tumors so-called Glioblastomas are so aggressive that patients between ages 40 to 64 have only a 5.3% chance with a 5-year survival rate. In addition, it mostly depends on treatment course procedures since 331 to 529 is median survival time that shows how this class is commonly severe form of brain cancer. Unfortunately, a mean expenditure of glioblastoma costs 100,000$. Due to high mortality rates, gliomas and glioblastomas should be determined and diagnosed accurately to follow early stages of those cases. However, a method that is suitable to diagnose a course of treatment and screen deterministic features including location, spread and volume is multimodality magnetic resonance imaging for gliomas. The tumor segmentation process is determined through the ability to advance in computer vision. For instance, CNN (convolutional neural networks) demonstrates stable and effective outcomes similar to one of other automated methods in terms of tumor segmentation algorithms. However, I will present all methods separately to specify effectiveness and accuracy of segmentation of tumor. In addition, widely recognized techniques based on GANs (generative adversarial networks) have an advantage in some domains to analyze nature of manual segmentations today. In this thesis, first section examines Fuzzy C-means (FCM), Atlas-based, Markov Random Fields (MRF), and Support Vector Machines (SVM) algorithms as a part of classification and clustering methods for brain tumor segmentation. Second section explains deformable model methods that include Parametric deformable models and Geometric deformable models. In third section, trilinear interpolation algorithm techniques apply image Pre-processing, Morphological Operation and Otsu Method for 3D MRI Brain image processing. In final section, we discuss the term Magnetic Resonance (MR) based on medical technology representing realistic images but different from original images. The Progressive Growing of GANs (Generative Adversarial Networks) and a large diversification of the GAN training method can determine the art of brain tumor segmentation in terms of the results of MRI (Magnetic Resonance Imaging) and the evaluation of proposed GAN method. GAN is suggested for brain tumor segmentation

as it may achieve the high achievable and competitive performance of networks which was proven in the BRATS 2020 database. Our ultimate goal is on this ongoing

operation to show that the GAN-based method could follow future reasonable trends and promising results in not only brain tumor detection but also other possible MRI related medical models.

### 1.1. Brain Tumor Segmentation Methods

Today, three major categories can explain brain tumor segmentation based on different principles and degree of human interaction requirements. These include semi-automatic, fully automatic and manual segmentations [1]. Firstly, semi-automatic brain tumor segmentation consists of software, interaction and user. The realization of tumor segmentation algorithms is a target area for software computing. The interaction covers the adjustment of segmentation information between the software and the user. For user case, it provides feedback response and visual information for software computing, but it requires to input some parameters before processes. Moreover, three processes of semi-automatic segmentation include feedback response, evaluation and initialization. One of the disadvantages of this segmentation category is to obtain same user at different times or different results from different experts. However, semi-automatic segmentation shows better results in comparison to manual segmentation. On the other hand, fully automatic brain tumor segmentation algorithm is a combination of prior knowledge and artificial intelligence. It is more likely to stimulate human intelligence to develop machine learning algorithms, but this method helps the computer analyze brain tumor segmentation without human interaction.

The manual brain tumor segmentation paints the regions of anatomic structure by using various labels and it draws the boundaries of brain tumor [1]. In this case, anatomy as a representation of brain tumor images should be studied by brain tumor experts, but most of the time manual segmentation yields poor results due to error-prone and time-consuming issues. This is because the more brain tumor images in the clinic are emerging, the more errors occur for the experts. The solutions are semi-automatic and fully automatic segmentation methods which address such problems directly in an advanced way. In contact, these two segmentation methods exhibit partial-volume effects and irregular boundaries with discontinuities for tumor images. Currently, alternative three categories are proposed through MRI-based methods for brain tumor

segmentation in order to solve challenges faced by semi-automatic and fully automatic brain tumor segmentation images.

## 1.2. Literature Review

MR imaging is a valuable detector of brain tumors in terms of size, type, shape and position. MRI scan detects fatal brain tumors known as glioma and meningioma without harmful radiations for patients. Early stages of these dangerous tumors can be easily diagnosed through multiple medical applications in order to cure further serious damages. According to World Health Organization (WHO), physicians classified tumors in four grades including grade 1, grade 2, grade 3, and grade 4. In first two grades, they detect meningioma as a lower level tumor. However, grade 3 and grade 4 examine glioma as one of more sever tumors. The study found that meningioma is about 20% of the brain tumors with a spherical shape and slow growth rate. Despite a low growth rate and low risk of the meningioma, it should be cured in early stages due to permanent damages for any patient in long term.

MR image analysis and interpretation processes can be complicated, sensitive and time consuming if color intensity for the lesions in brain tumors describes many variations and size of lesions are not detectable. For that reason, surgeons and neurologists must be responsible on correct decision making in order to analyze promising methods for misinterpretations in MRI scans. These methods can be quantitative image detection techniques in dealing with such misleading and imperfections.

Paul et.al suggested convolutional neural networks (CNN) for the dataset for brain tumor classification. Three classifiers were examined for images including fully connected neural network, random forest and convolutional neural network. CNN showed 90.26% accuracy rate with two convolutional layers and two fully connected layers with 800 neurons. MaxPool layers follow the convolutional layers with 64 filters of 5x5 size whereas SoftMax layer follows the output layer containing three neurons as the number of classes.

Abiwinanda et al. applied CNN with two convolutional layers of 3x3 size and 32 filters by using a fully connected layer of 64 neurons. The accuracy rate was 84.19% on this dataset. On the other hand, the features were extracted from CNN and employed with a Kernel ELM classifier. The accuracy rate was 93.68%. Anaraki et al. investigated

CNN architecture using a genetic algorithm to evolve the results and accuracy rate for this method was 94.2%.

Abdel-Qader and Ismael examined 90 neurons for a hidden layer, 3 neurons for an output layer, 270 inputs for a neural network with 91.9% accuracy rate by extracting statistical features from MR images. Tahir et al. improved the outcomes of statistical models and determined multiple preprocessing methods for classification. 86% accuracy was reported for Support Vector Machines (SVM) used to standardize the model.

Zhou et al. investigated resolution of slice labeling through LSTM based network as a purpose of a sequence of images in MRI scans. LSTM and autoencoder enable features to be extracted from classified scans and axial view respectively. The report on this dataset shows 92.13% accuracy rate. Despite the fact that selected slices in this dataset are only a component of the main dataset, some zero matrices are added to each image for evaluation.

Afshari et al. employed Capsule Net to classify three tumor types for MR images by using default architecture. Segmented tumors and raw brain images presented 86.56% and 72.13% accuracy rate for classification respectively. The final accuracy in early phase and better results for network in these processes were questionable and undefined due to stopped learning phase after ten epochs. The second paper proposed by Afshari et al. introduced the position of the tumor using Capsule Net for MR image with 90.89% accuracy rate. Moreover, Phaye et al. applied various capsule network architectures using CapsNet on the dataset with 95.03% accuracy rate. Cheng et al. examined gray level covariance matrix, intensity histogram and bag of words as a part of three feature extracting methods with accuracy rate of 91.28%.

## 1.3. The problem of the study

The problem of the study is a solution for curing brain cancer in its first stages without permanent damages to the patient in a long term. If not treated and cured in early stages, it can cause the death for a large number of patients and some of them can get harmful ionizing radiations. Moreover, most researchers investigate brain tumor segmentation algorithms, but not the feature extraction. In this case, it is better to consider types of brain tumors in actual applications and variance in appearance of

various brain tumor grades. The experience in feature extraction for brain tumor would potentially improve validity, accuracy, and robustness of tumor segmentation based on MR images.

## 1.4. Methodology

In this thesis, most of brain tumor segmentation methods provide the possibility of getting high accuracy rate and reliability for a deep learning for tumor classification in magnetic resonance images (MRI). First, semi-automatic, fully automatic and manual segmentations are presented to explain fundamental realization of tumor segmentation algorithms. Then, preprocessing operations and imaging modalities based on MRI brain tumor segmentation are introduced in terms of classification and clustering method, as well as deformable model methods. In addition, another image detection technique known as trilinear interpolation algorithm for 3D MRI brain images were proposed by five major steps to construct 3D image from 2D MRI human cortex images. Finally, we present generative adversarial networks (GAN) to achieve a well-defined image resolution for medical imaging. In this part, the deep details network by modalities including T1, T2, T1c, and FLAIR are generated through BRATS2020 dataset. Furthermore, two GAN-based approaches (DCGAN and WGAN) and results with GAN pre-train on both introduced split and random split were evaluated to better learn the structure of MR images for brain tumor segmentation based on provided datasets.

## 1.5. Database

The database contains 371 brain MR images in total and four modalities of MR images (T1, T2, T1c, and FLAIR). The dataset of these modalities is from 2018, 2019, 2020 Multimodal Brain Tumor Image Segmentation Benchmark (BRATS) challenges. Another database mainly includes 3064 T-CE MR images with 1426 glioma images, 708 meningioma images, and 930 pituitary tumor images proposed by Cheng et al.

# CHAPTER 2

## Classification and clustering methods

Due to the practice of radiology by radiologists, making accurate decisions and learning patterns from empirical data or learning complex relationship can be studied by providing machine learning that simplifies the diagnosis and anaylsis for medical images [2]. In medical practice, unsupervised, semi-supervised and supervised learning are essential categories of classification and clustering methods based on different principles and utilization of labels of training samples. Unsupervised learning algorithm contains no label information and only one set of observations for each sample. Obviously, latent variables and a set of unobserved variables cause such features and observations. The main objective of the unsupervised learning is to reveal the latent variables and to determine relationship between samples between samples and behind the observations respectively. Hence, clustering algorithm explains unsupervised learning effectively. Semi-supervised learning explores a combination of unsupervised and supervised learning algorithms. Due to having high costly labeling of data and being inapplicable for some applications semi-supervised learning was targeting the development of its algorithms [3]. Indeed, it has an advantage in terms of using unlabeled and labeled data in the training process. In addition, supervised learning algorithms study two major parts which include output observations (called as effects) or labels and input observation (called as causes) or features. Supervised learning shows a functional relationship which is a set of numerical coefficients and equations from training data. This data generalizes given procedures to testing data so that classification algorithm effectively explains supervised learning as a representative method. Classification or clustering methods in brain tumor segmentation include Fuzzy C-means (FCM), Atlas-based algorithms, Markov Random Fields (MRF), and Support Vector Machines (SVM).

### 2.1. FCM algorithms

Pattern recognition is commonly used area for FCM method which corresponds to each cluster center between the data point and the cluster on the basis of distance issue, but before it assigns membership to each data point [4]. Getting high possibility of membership towards the cluster center depends how nearer the data is to the cluster center. Getting encouraging results of MR data, getting satisfactory results better than

k-means algorithm and better for overlapped data set, assigning membership of data points to not only one cluster center in which most data point exclusively belongs to one cluster center not similar to k-means are significant advantages of FCM algorithm.

Brain tumor segmentation is divided into tissue classes which generate segmentation images in order to demonstrate neuropathological and neuroanatomic issues by generating contrast information from raw MR image data. Necrotic core, active cells and unsupervised FCM clustering algorithm used edema are included in these classes. Furthermore, the integration of multispectral histogram analysis and knowledge based methods enables MRI images to determine segmentation of brain tumor [5]. Fuzzy clustering as a knowledge-based method is an alternative procedure for MRI images of brain tumor segmentations. It is also used to build the tumor shape based on 3-D connected components. In addition to fuzzy knowledge and modified seeded region growing, a segmentation method which is so-called Fuzzy Knowledge-based Seeded Region Growing (FKSRG) shows effective segmentation results for multispectral MR images compared to segmentation of functional MRU with Brain Automated Segmentation Tool.

The FCM is considered as an iterative algorithm which is very time consuming clustering method. In fact, Fast Generalized FCM (FGFCM) and Bias-Corrected FCM (BCFCM) algorithms are major solutions to decrease possible execution time in advance. FGFCM clustering algorithms are considered as robust FCM framework for segmentation of brain tumor [6]. While BCFCM is a time-efficient algorithm in terms of providing brain images with good quality segmentation. In this method, supporting virtual brain endoscopy is a process obtained effectively by this algorithm in order to better analyze brain tumor segmentation.

A modified FCM-based method determines fast and accurate segmentation aiming to decrease sensitivity issue of standard FCM algorithm. For that reason, this method was proposed for mixed noises including impulse, intensity non-uniformity and Gaussian noises. Moreover, this method uses context based dependent filtering technique to better realize gray and spatial level distances. In this case, first step is extraction of a scalar feature value through neighborhood of each pixel. The next procedure is an observation of enhanced FCM algorithm regarding histogram-based approach connected with clustering process. Most researchers study a neighborhood attraction concept depending on features and relative location of pixels in order to develop the performance of FCM algorithm. However, segmentation results depend on degree of

attraction in which determination of this process is difficult to obtain in most cases. The Genetic Algorithm (GAs) and Particle Swarm Optimization (PSO) have been introduced to reach optimal solutions [7]. PSO has no challenges in finding exact solutions while GAs show low performance for this issue. While the determination of the optimum value for degree of attraction is practically achieved through the combination of PSO and GAs. In addition to segmentation of brain tumor, the combination of fuzzy c-means and k-means algorithms are essential to determine the stage and size of tumor accurately. In contrast to the manual segmentation, this combination offers reproducibility and accuracy with tumor tissue segmentation that reduces time for the improvement of segmentation.

## 2.2. Atlas-based algorithms

Atlas-based algorithm is used to register various images, guide segmentation of brain tissue, and restrict tumor location. It is also used for generative classification models and three major steps are included in this algorithm. First of all, the atlas and the patient are added to global correspondence by assistance of an affine registration. Second, a template is introduced for brain tumor regarding seeding of a synthetic tumor into brain atlas. Third, brain tumor growth and optical flow principles explain seeded atlas deformation. Furthermore, researchers examine the tissue model through defining probabilistic information and imposing spatial constraints depending on atlases. Moreover, Expectation Maximization (EM) method is introduced to modify an atlas from different MRI modalities knowing that the information about tumor location is linked to the modified atlas with patient-specific information [8]. This procedure enables a probabilistic tissue model to be employed and brain tumor to be segmented. One of advantages of atlas-based methods is about better integration between domain knowledge and consideration of atlas-based segmentation. While it is challenging to account the variability of such prior information. In fact, lesion growth prior model shows radial expansion of lesion which comes from the starting point for brain atlas deformation. Obviously, this process results in better segmentation results of brain tumor by analyzing large space-occupying tumors. In a population, brain atlases contain averaging pre-segmented images which are equally constructed and these methods experience lower segmentation guidance capability and local inter-subject structural variability. In order to solve such problems a multi-region-multi-reference framework is a best alternative to consider for atlas-based neonatal segmentation of brain tumor. As a result of using a spatial regularization and generative probabilistic model, the combination of a latent brain tumor atlas and healthy brain atlas is an accurate determination of brain segmentation from multi-sequence images [9]. The

Figure 2-1 demonstrates the results of T1 and T2 brain tumor segmentation as a part of atlas-based segmentation of magnetic resonance brain images. The localization suggests multi-modal segmentation optic pathway gliomas to be used for classification with probabilistic tissue model based on brain atlas at a recent time. The effectiveness and practicability of atlas-based methods have a close relationship with the precise atlas. In Table 2-1, Talairach-Tournoux, Whole Brain, BrainWeb, and Brodmann are examples for atlases described as follows:

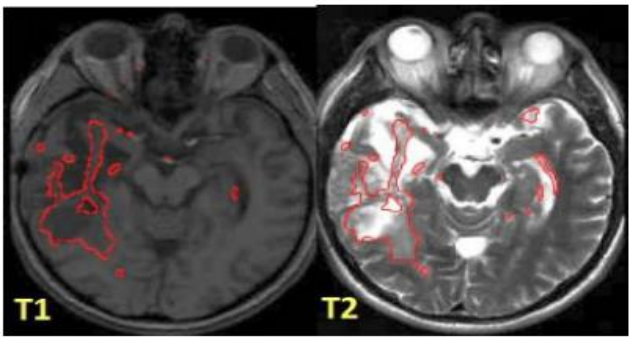


Figure 2-1. The results of T1 and T2 brain tumor segmentation

Table 2-1. The current existing atlases.

| **Name** | **Representation** | **References** |
|---|---|---|
| Brodmann | The first brain atlas | [10] |
| Talairach-Tournoux | Construct a three-dimensional coordinate to provide a standard space | [11] |
| BrainWeb | Widely used in the brain MRI images analysis | [12] |
| Whole Brain | Used in neurosurgery at Harvard Medical School | [13] |

## 2.3. MRF algorithms

These algorithms describe the integration of spatial information with classification or clustering process [14]. Overlapping and effect of noise are possible issues that have been reduced by adding MRF in clustering methods. If the neighbor of labeled region is the same, MRF will determine this process by the fact that the region is strongly labeled (non-brain tumor or brain tumor). Sequence data is labeled and segmented through building probabilistic models using Conditional Random Fields (CRF) [15]. Both MRF and CRF provide high accuracy for segmentation of brain tumor results by representing complex dependencies among data sets. GMM as an example of the mixture model can model different tissues including Necrotic Core (NC), Edema (E), GM, WM, Active Cells (AC) and CSF. This model uses Iterated Condition Modes (ICM) algorithm to train the MRF [16]. Each tissue can be segmented by different models of different tissues. A multi-layer MRF framework can easily detect brain abnormalities so that such layers include input, structural coherence, region intensities, and spatial locations [17]. Moreover, it is clear that a change in high-level classification depends on a given voxel which is correlated with strong similarities shared by the attributes of lower-level layers. Spatial accuracy-weighted Hidden Markov random field and Expectation maximization (SHE) provides better quality of tumor segmentation in terms of enhanced-tumor and automated tumor segmentation. In clinical applications, high-resolution images are commonly determined together with low-resolution sequences. The process of tumor segmentation follows multi-channel MR images using different resolutions through incorporation of the optimization procedure of the Hidden MRF (HMRF) with the spatial interpolation accuracy of low-resolution images proposed by SHE. Consequently, SHE algorithm presents more accuracy for the results of tumor segmentation. In case of an automatic method, brain tissues are segmented based on non-rigid registration of an average atlas which is combined with a biomechanically justified tumor growth model. It aims to detect causality of tumor mass-effect in a way to simulate soft-tissue deformations. Correspondence between the patient image and the atlas is the process provided by the tumor growth model which is considered and formulated as mesh-free MRF energy minimization problem before registration step. Compared to other approaches, tumor growth model is fast, simple and non-parametric due to maintaining similar accuracy. An automated hierarchical probabilistic framework supported through the use of an adapted MRF framework and multi-window Gabor filters enables brain tumors to be segmented from multispectral brain MRI [18]. BRATS database in the framework assists segmentation of brain tumor as edema and non-edema. The Figure 2-2 shows how labels of algorithm correspond to labels of expert closely.

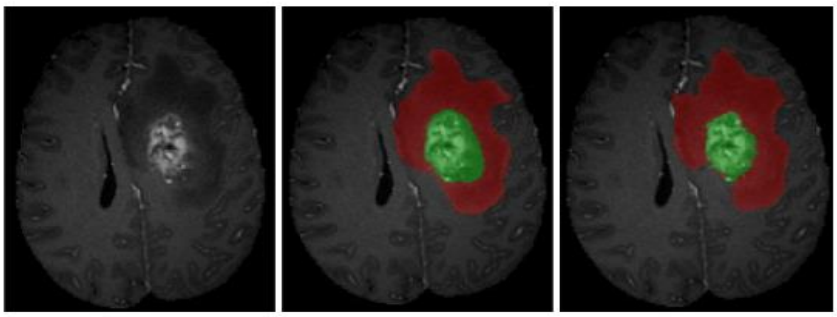

a b c

Figure 2-2. (a) unlabeled TIC slice; (b) expert labelling; (c)algorithm labels (red – edema, green – non-edema) [96]

## 2.4. SVM algorithms

Vladimir N. Vapnik invented the original version of SVM algorithm, but Cortes and Vapnik in 1993 studied current standard incarnation [19]. To deal with supervised classification issues, a parametrically kernel-based method was proposed as SVM and brain tumor segmentation was a commonly known field for SVM algorithms [20]. One-class SVM examines the ability to learn the nonlinear distribution of image data which uses no prior knowledge [21]. It is also applicable to achieve better segmentation results by following an implicit learning kernel and automatic procedure of SVM parameters training. These results support the extraction of brain tumors for better segmentation results compared to fuzzy clustering method. The researchers were willing to build voxel-wise intensity-based feature vectors via a high number of MRI modalities classified by SVM [22]. The healthy tissues and also sub-compartments of healthy and tumor regions are segmented by this method, but similar approach based on SVM used a lower number of modalities and segmented one tumor region [23]. The feature selection with kernel class was introduced to improve this method and it showed better results. In order to segment the brain tumor from multi-sequence MRI images a fusion process and a multi-kernel based SVM in collaboration with a feature selection was offered as an alternative. Ameliorating the contour of tumor region (use of the

distance and the maximum likelihood measures) and classification of tumor region (use of a multi-kernel SVM) are major two steps of

a multi-kernel based SVM integrated with fusion and feature selection processes. In addition to classifying the tumor region, this step focuses on the performance of multi-image sources and multi-results. The accuracy and diminution of total error are expected results obtained through this method compared to traditional version of single kernel SVM. A fully automatic method was also essential to define segmentation of brain tissue which used multispectral intensities for SVM classification as a combination [24]. This method textured with hierarchical approach (specifically, subsequent hierarchical regularization) based on CRF to get acceleration and robustness. Thus better results and accuracy can be achieved by different levels of regularization at various stages. The Figure 2-3 denoted potentially useful effects of SVM algorithms for MRI images in segmentation of brain tumor. The Table 2-2 explains the relatively good methods and their presentations of MRI-based brain tumor segmentation.

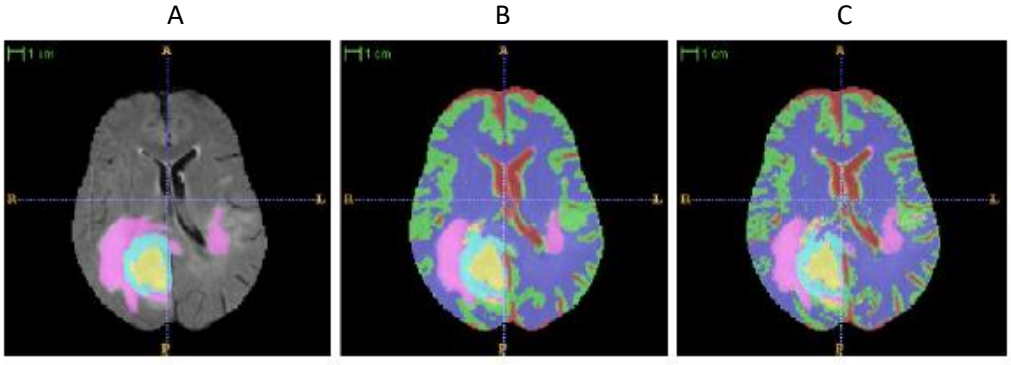


Figure 2-3. (a) manual segmentation; (b) hierarchical SVM-classification with CRF-regularization; (c) non-hierarchical SVM-classification without regularization.

Table 2-2. Some good algorithms based on MRI brain image segmentation.

| **Method** | **Presentation** | **References** |
|---|---|---|
| Combination of k-means and fuzzy c-means | Better accuracy and reproducibility | [25] |
| FKSRG | Lower over- and under-segmentation | |

| | | |
|---|---|---|
| Multi-region + multi-reference framework | Higher tissue overlap rates and lower standard deviations | |
| Generative probabilistic model + spatial regularization | Improvement over the traditional multivariate tumor segmentation (25 glioma) | [9] |
| Probabilistic model + localization | More robust applied to monitor disease progression | |
| Non-rigid registration + atlas + MRF | Multivariate tumor segmentation | [9] |
| SVM + CRF | 10 multispectral patient datasets more detail segmentation low computation times | [24] |
| Decision Forests + tissue-specific Gaussian mixture models | Segmenting the individual tissue types simultaneously such as AC, NC, E, etc. | [26] |
| SVM + Kernel feature selection | Good results tested in T1w, T2w and T1c, low computation time | [27] |

# CHAPTER 3

## Deformable model methods

Parametric and geometric deformable models are major components of model-based segmentation methods that can handle the issue of the appearance of 3-D MRI data with respect to extraction of boundary elements which belong to same structure and integration of those elements into a consistent and coherent structure model. In most cases, such issues are challenging to be segmented through simple methods compared with combination of SVM classification techniques which demonstrate high accuracy and diminution of total error. The capability of segmenting images of anatomic structures helps to determine resistance of deformable models. This segmentation exploits constraints about size, shape and location of anatomic structures which stem from image data with a prior knowledge. Deformable models are highly adjustable for the variability of biological structures in terms of various individuals [28]. In addition to deformable models, they are more likely to assist clinicians and medical researchers through intuitive interaction mechanisms in order to determine necessary model-based image interpretation task.

### 3.1. Parametric deformable models

These models were so-called active contour models and snakes in some periods. After introduction of snakes in 1988, they are used to locate object contours including appropriate initialization in practice [29]. The snakes are capable and sensitive to detect the boundary of brain tumors that is highly significant as a step of brain tumor segmentation in parametric deformable models. According to studies done about the resolution of the boundary, the snake technique shows more effective results compared to conventional edge detection including Canny, Sobel and Laplacian algorithms. However, the snake function in homogeneous regions is positively obtained while it is zero at the edges. Therefore, the improvement of brain tumor segmentation results on T1 brain tumor MRI was achieved using the balloon model and the Gradient Vector Flow (GVF). GCF aimed to analyze inability and short capture range which stem from the traditional snakes to track concavity of boundary. Moreover, the spatial relations as refinement step enable a parametric deformable model to estimate boundaries of any type of brain tumors accurately which is on T1 MRI [30]. The growth of snakes capture range can be defined by the balloon model apart from the parametric deformable

model. The combination of deformable registration and segmentation of brain scans was proposed based on Expectation Maximization (EM) algorithm to a normal atlas in a way to explain incorporation of atlas seeding and a glioma growth model. This process studies modified atlas which represents the normal atlas into one with edema and a tumor. In addition, utilization of the posterior probability estimation of different tissue labels and registration into the patient space are essential characteristics of the modified atlas. The Expectation Maximization algorithm is highly optimistic to refine the posterior probabilities of tissue labels, the tumor growth model parameters and the estimates of registration parameters. It is also necessary to note that manual location of initial position of the parametric deformable model demonstrates avoidance of converging to wrong boundaries if it is close to desired boundary.

### 3.2. Geometric deformable models

Geometric Deformable Models (GDM) is sometimes known as level sets which improves topological changes for merging of contours and splitting processes. In fact, these procedures are more challenging to be handled naturally in terms of topological changes when using segmentation of 3D MRI data through parametric deformable models [31]. In most cases, segmentation methods of brain tumor cannot be easily achieved in practice when dealing with regularly shaped objects. On the other hand, the issue stems from improvement of initialization of parametric active contours and symmetrical placement of initial contour with respect to boundaries of interest. Level-set snakes were highly preferable to gain an advantage compared to mathematical morphology and conventional statistical classification, because snakes experience careful initialization which have constant propagation and leak through missing boundary parts. A knowledge-based segmentation algorithm combines level-set snakes and pixel-intensity distribution that present more precise boundaries. Some researchers examined a deformable model using a Charged Fluid Framework (CFF) to aim brain tumor segmentation for a certain period of time [32]. However, CFF was extended and modified for brain tumor segmentation by proposing the Charged Fluid Model (CFM). Brain tumor can be segmented in a variable level set formulation by proposing a region-based active contour model. This model suggested that the image intensities were approximated on two sides of contour by two fitting functions originated from data fitting energy. A regulation term as a part of the level set formulation shows derivation of a curve evolution which potentially targets energy minimization. The level set regularization term preserved regularity of level set function in a way to eliminate

expensive re-initialization. In this case, the progress of level set function depends on accurate computation of the level set regularization term. A few researchers determined a local clustering criterion function which is specified for intensities considered in a neighborhood of each point. However, a local intensity clustering property was also studied through brain tumor and other images with respect to intensity inhomogeneities. Integration of the local clustering criterion supports an energy functional over the neighborhood center in order to convert to formulation of the level set. Estimation of bias field and level set evolution with an interleaved process lead to minimization of the energy [33]. Combination of tumor segmentation and level set including tumor probability was achieved by a tumor-cut algorithm which resulted spatial smoothness.

To sum up, FCM, ANN and MRF are commonly used algorithms in terms of deformable model analysis. This method can aim the accuracy of brain tumor segmentation by incorporating two or more algorithms. Therefore, brain tumor segmentation has a direct effect on medical image analysis for surgical planning that is most important issue in term of validity of segmentation process. As a part of tumor segmentation, commonly applied evaluation standards include Dice Similarity Coefficient (DSC) and Jaccard coefficient which range from 0 indicating no overlap to 1 indicating perfect overlap. Moreover, probabilistic brain tumor segmentation was analyzed through three following validation metrics; Mutual Information (MI), Dice Similarity Coefficient (DSC) and the Receiver Operating Characteristic curve (ROC). These methods aim to sustain tumor monitoring, a preliminary judgment on diagnosis as well as the physician with therapy planning.

# CHAPTER 4

## Trilinear Interpolation Algorithm Techniques for 3D MRI Brain Image.

There are many diagnosis and detection imaging techniques for treatment of potential risks caused by brain tumor diseases. Computed Tomography (CT), Scanner, Position Emission Tomography (PET) and Magnetic Resonance Imaging (MRI) are commonly used diagnostic imaging tools to practice for tumor segmentation [63-65]. In recent year, researches show that the process of obtaining 3D images from 2D medical images becomes increasingly necessary to determine an appropriate identity and regional development of tumors. Moreover, Machine Cube supports 2D CT image constructed 3D spine image or 3D surface of knee [34]. In this method, data blocks are divided into cubes that were made up of eight adjacent voxels. By using the triangular mesh material surfaces were constructed from there eight adjacent voxels. As a result, simple construction operations, 3D image production with high resolution and fast calculation are advantageous procedures experienced through this method. If the large number of 2D image data is processed, the calculation process slows down. In most cases, noise occurred due to images captured from sensor should be reduced by pre-processing 2D images in order to construct the 3D image with high quality of improvement. Therefore, a mean-unsharp filter is able to increase filtered noise and high frequency components. Before low-level image separation the intensity values of grayscale image may process the growth method of MRI images. In this case, low-contrast images can be easily changed to higher-contrast images. Furthermore, making the tumor boundary depends on how morphological operations are utilized in order to stretch and fill a possible object for segmentation process. In this section, we will determine Otsu method for constructing 3D image with a support of segmentation of 2D images by finding the gray level threshold values.

On the other hand, segmentation method can be jointly connected with the algorithm of regional development with respect to similarity of adjacent pixels related to the nuclear point. Choosing the error and nuclear initial point which depend on between neighboring pixels and nuclear point can be defined as a result of combination of

algorithm. Practically, the acquisition of 2D medical image may process noise on it, but Otsu technique as a threshold of traditional method segment some of the areas required for 3D image development. According to some research studies done on Otsu

method, it may not often demonstrate better results. Instead, dividing 2D image into many layers by Otsu method with multilevel may provide better and efficient results. Pixels in 2D image are combined with region development algorithm to process segmentation of the image in which pixels have same regions [35]. The process may continue until the 2D image reaches coordinate axes (x, y, z) after segmentation. The calculation of approximate value of a point allows to construct the 2D image surface between two consecutive layers which are represented in the spatial domain. In fact, the linear interpolation approves this construction of 2D image surface before calculation of a value of the point.

Binh Duong General Hospital provided dataset for construction of 3D image by considering 44 2D MRI brain images with 256x192 pixels. There are some major following steps to describe the construction of 3D image from 2D MRI human cortex images. First step is to re-process 2D image including image enhancement and noise rejection. Second step is to employ morphological operator and eliminate pixels in 2D images around object boundaries. Third step is called Otsu method or image segmentation where segmented and pre-processed images for 3D construction separate the brain area from the cortex. Final step is to construct 2D images after the segmentation to obtain 3D image by using a trilinear interpolation algorithm (also known as 3D image construction).

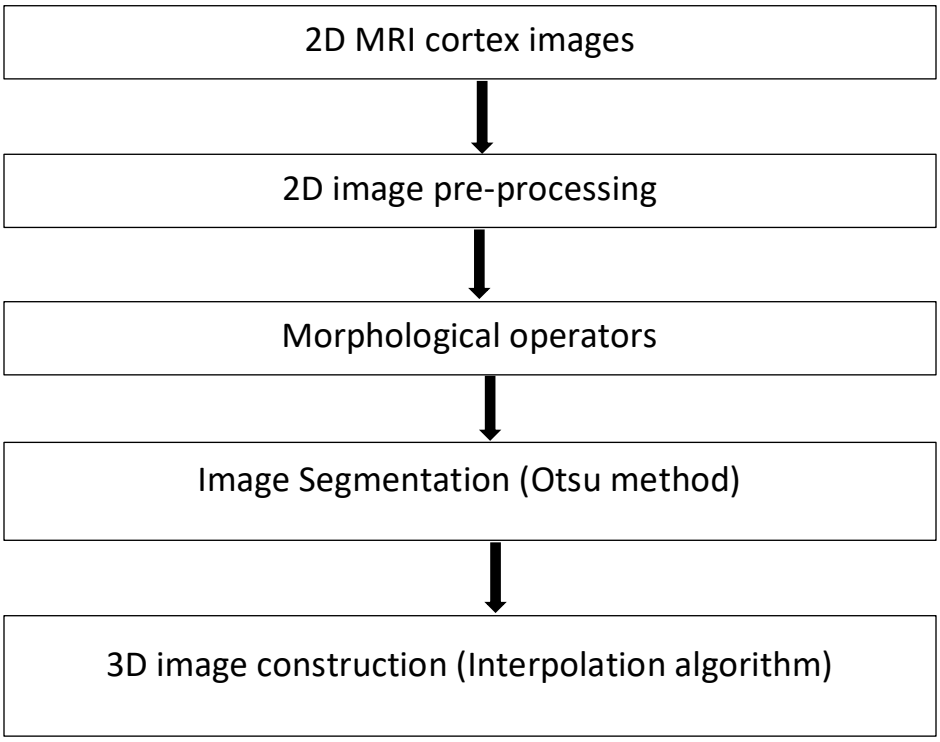


### 4.1. Image pre-processing

Image pre-processing follows an average filter process to smooth 2D MRI images with noise in order to construct 3D image. The equation (1) below describes elimination of noise by applying the average filter that is convoluted with each 2D MRI image.

$$r(x,y) = \frac{1}{ab} \sum_{s=-a}^{a} \sum_{t=-b}^{b} w(s,t) f(x+s, y+t) \qquad (1)$$

- r(x,y) is output image after the process of filtering;
- w(s,t) is axb filter window.

In Figure 4-1, the average filter with a 3-by-3 kernel after convolution is given as the result of 2D MRI cortex image $\frac{1}{9}\begin{pmatrix} 1 & 1 & 1 \\ 1 & 1 & 1 \\ 1 & 1 & 1 \end{pmatrix}$.

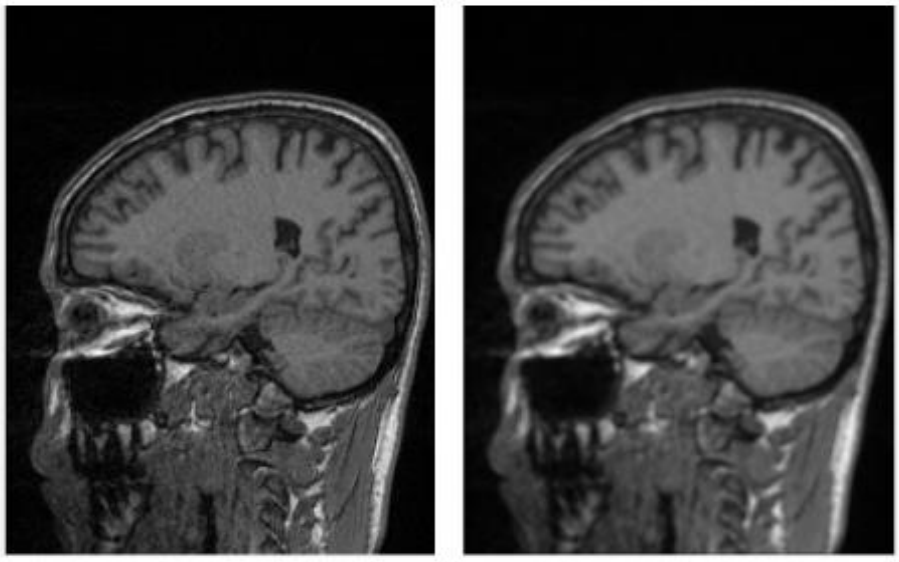

1 2

Figure 4-1: (1) Original human cortex image; (2) Cortex image after the mean filter.

After separation of complete brain region form the cortex image, the convoluted image provides smoother processing results in terms of using mean filter compared with using the median filter.

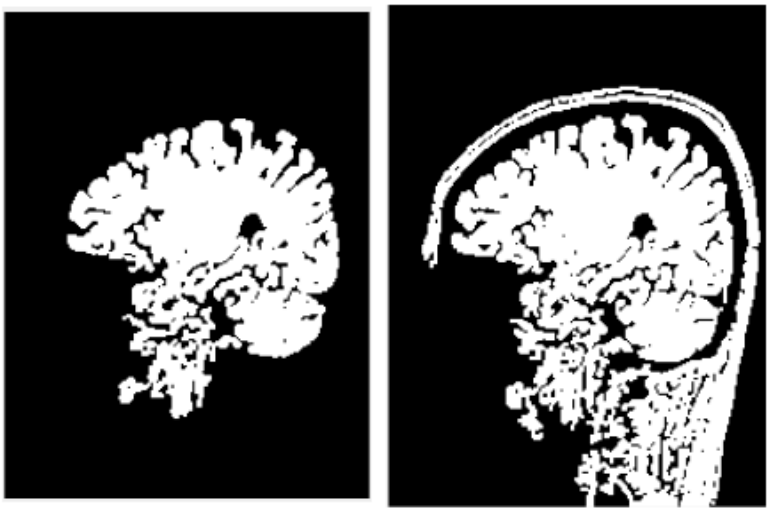

1 2

Figure 4-2: (1) Image after using the mean filter; (2) Image after using the median filter.

In Figure 4-3, not only enhancement of image with high frequency components but removal of low frequency components may be realized through application of unsharp filter with 3x3 size.

$$\frac{1}{2}\begin{pmatrix} -1 & 0 & -1 \\ 0 & 6 & 0 \\ -1 & 0 & -1 \end{pmatrix} \quad (2)$$

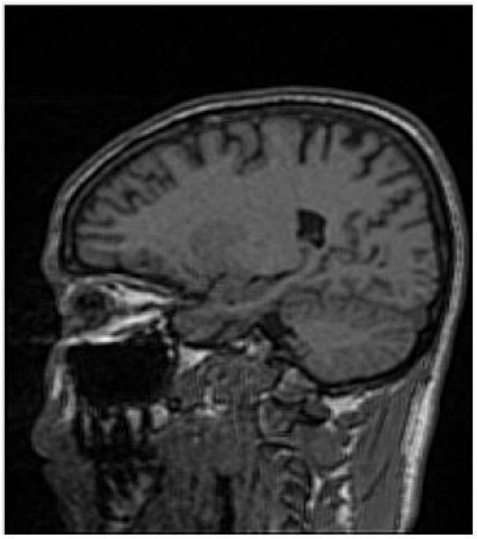

Figure 4-3 : 2D MRI cortex image after the unsharp filter

Moreover, image enhancement is a solution to make object better on higher contrast in case of low contrast after image filtering. Spreading the pixel values in the image is a significant procedure to expect transformation of the higher contrast image when proposing a histogram equalization algorithm [36]. This algorithm uses a special equation (3) to enhance the image as follows:

$$p_r(k) = \frac{n_k}{MN} \qquad (3)$$

- nk is the number of pixels observed at the kth gray level in terms of the input image;
- MN is total pixels of the image;
- Pr(k) denotes the probability density function in the image connected with the kth gray level values.

Apart from probability density function (PDF), the calculation of the output expression of the image is defined:

$$s = (L-1)\sum_{j=0}^{k} p_r(j) \qquad (4)$$

- L denotes the number of gray levels in the image;
- S(x,y) denotes the number of the pixels with respect to output image at the kth gray level.

In Figure 4-4, first image represents before enhancement issue which uses unsharp filtering process. While, second image clearly shows after enhancement procedure. Nevertheless, the histogram equalization stimulates unsharp image with high frequency components to be enhanced for creation of higher contrast. Hence, Figure 4-5 (1 & 2) demonstrates representation of images where image before enhancement experiences the large number of pixels with distribution of being closed to the zero point. However, image after enhancement offers the histogram equalization with pixel values spreading on gray level axis.

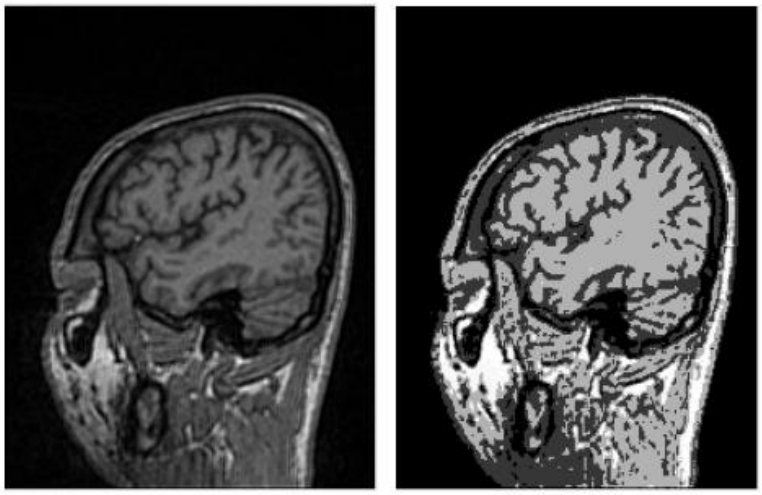

1 2

Figure 4-4: (1) Image using the unsharp filter; (2)Image after enhancement.

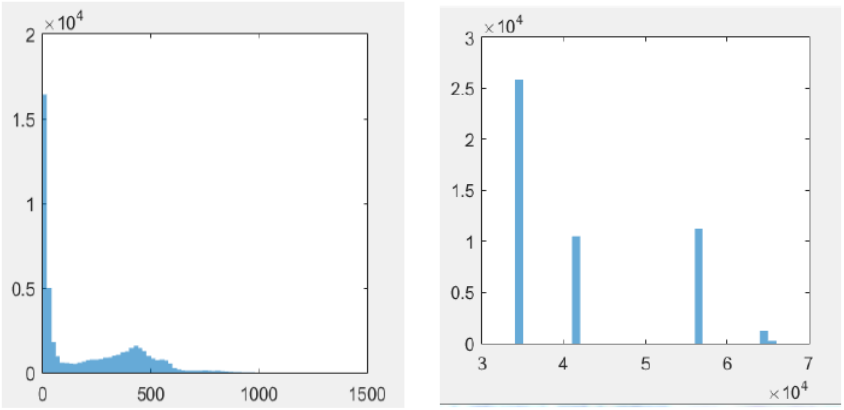


1 2

Figure 4-5: (1) Image before enhancement; (2) Image after enhancement using the histogram equalization

## 4.2. Morphological Operation

The enhanced image continues the process for image imperfection after filtering 2D MRI cortex image, but this filtering removes noise and enhances the image. As a result of the image enhancement, a morphological algorithm removes a few unnecessary parts around objects for the image. Only potentially important object is remained for 3D

image construction by morphological algorithm. In addition, Dilation and Erosion are common operations of this algorithm in which the dilation operator considers structures and shapes of 2D image enhancement. At this moment, the morphological operation removes the undesired parts and combines boundaries around the objects. On the other hand, the morphological image determines the convolution between a kernel and the input image for image calculation as given below:

$$m(x,y) = max \begin{cases} s(x-i, y-j) + h(i,j) \\ |(x-i), (y-j) \in D_s, (i,j) \in D_h \end{cases}$$

- h(i,j) is a kernel with the size of 2x2 matrix
- Ds and Dh are the domains of s image and k kernel.
- S(x-i,y-j) denotes output images.
- M(x,y) denotes input images.

In Figure 4-6, the matrix of the 2x2 kernel is structured as follows:

| | |
|---|---|
| 1 | 1 |
| 1 | 1 |

Figure 4-6

In Figure 4-7 (2), the dilation operator in morphological algorithm enlarges the boundaries of object regions when producing the 2D MRI cortex image. For this reason, image after morphological operation combines the boundaries of object regions and provides better results compared with the enhanced image given as in Figure 4-7 (1).

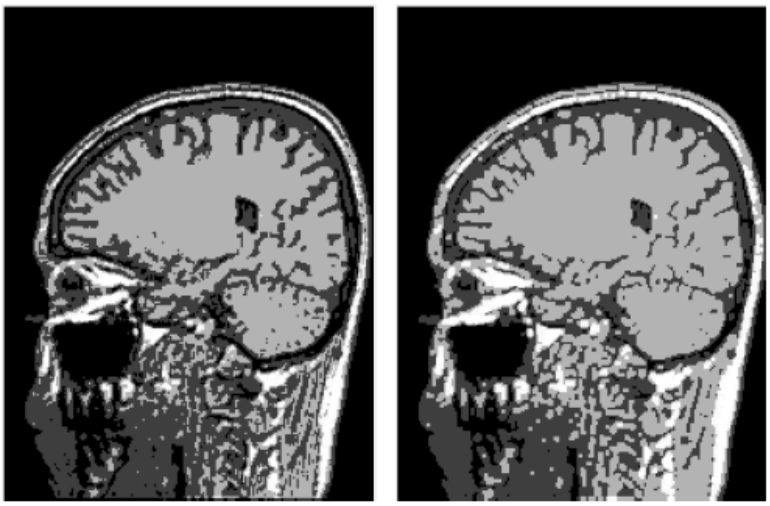

1 2

Figure 4-7. (1) Representation of the enhanced image; (2) Image after the morphological operation.

### 4.3. Image Segmentation using Otsu Method

Otsu algorithm is employed for calculation of many gray level thresholds which determines 2D MRI image segmentation before construction. The threshold value in this particular algorithm is selected corresponding to minimum variance within the class. The segmentation algorithm equation (6) in terms of the set of 2D MRI cortex images can be shown as given;

$$\sigma_B^2 = \omega_0(\mu_0 - \mu_T)^2 + \omega_1(\mu_1 - \mu_T)^2 \qquad (6)$$

$$\omega_0 = \sum_{q=0}^{k-1} p_q(r_q) \qquad (7)$$

$$\omega_1 = \sum_{q=k}^{L-1} p_q(r_q) \qquad (8)$$

$$\mu_0 = \sum_{q=0}^{k-1} \frac{q p_q(r_q)}{\omega_0} \quad (9)$$

$$\mu_1 = \sum_{q=k}^{L-1} \frac{q p_q(r_q)}{\omega_1} \quad (10)$$

$$\mu_T = \sum_{q=0}^{L-1} q p_q(r_q) \quad (11)$$

$$p_q(r_q) = \frac{n_q}{n} \quad (12)$$

where Pr(rq) is the probability density function of image histogram, $r_q$ and L is the maximum gray level of the image, ω0 and ω1 denote the background and foreground variances, $n_q$ describes the total number of pixels with gray level, and n is the total number of pixels in the image.

In Figure 4-6 (2), traditional Otsu method is applied for 2D cortex image after segmentation from morphological image. Otsu method in segmentation provides quick segmented image using 7 thresholding, but the segmentation almost depends on a threshold aiming to minimum variance. In some cases, this procedure can result undesired object with some lost parts corresponding to the segmented image as shown in Figure 4-8.

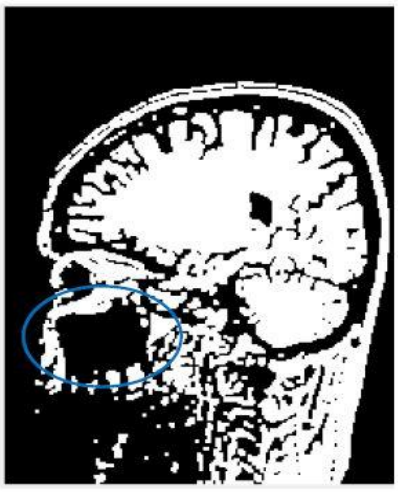

Figure 4-8. MRI cortex image segmentation with traditional Otsu method with the 7 thresholding.

Similar to Figure 4-8, same Otsu method is proposed to segment the spine image and Figure 4-9 demonstrates some lost parts of object in the image. Obviously, traditional Otsu method supports better outcomes of constructing the 3D images choosing a threshold for segmentation which will enhance for diagnosis of doctors.

1 2

Figure 4-9. (1) Original image; (2) Image after the traditional Otsu segmentation.

An Otsu method also utilizes multilevel to remove unnecessary parts in the image and retain the whole desired objects before 3D image construction. An equation (13) expresses the Otsu segmentation with two thresholding multilevel as follows:

$$\{t_1^*, t_2^*\} = arg_{1 \le t_1 < t_2 < L} max\{\sigma_B^2(t_1, t_2)\} \quad (13)$$

where t1* and t2* are two thresholds based on maximum variance within the class.

In Figure 4-10, traditional Otsu method is proposed for 2D MRI cortex image to simulate the result of image segmentation with two thresholds, but this image describes the mouth object more clearly compared to Figure 4-8.

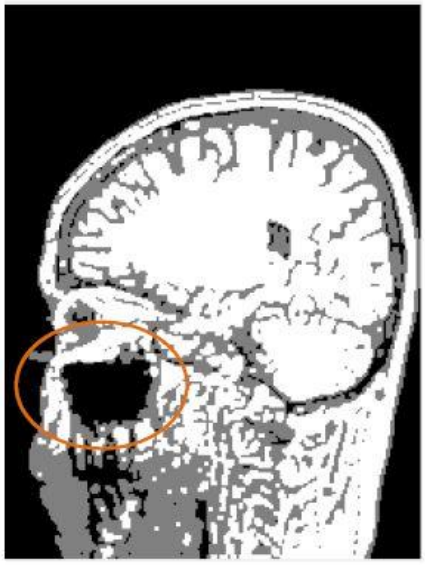

Figure 4-10. 2D MRI cortex segmentation with a support of Otsu method with two multilevel.

### 4.4. Interpolation Algorithm

A set of 2D images generates 3D brain image on a coordinate system after segmentation established to overlap in order. The 3D brain image enables to observe possible issues inside 3D brain part considering different angles. The calculation of pixels between two slices is realized through representation of a trilinear interpolation method as shown in Figure 4-11. This method assists to construct a typical object from a group of discrete points. A special equation (14) below provides the calculation of value in spatial domain (u, v, w) with respect to an approximate point of 2D images:

$$\begin{aligned} p_{uvw} = {} & p_{000}(1-u)(1-v)(1-w) + p_{100}u(1-v)(1-w) \\ & + p_{010}(1-u)v(1-w) + p_{001}(1-u)(1-v)w + p_{101}u(1-v)w \\ & + p_{011}(1-u)vw + p_{110}uv(1-w) + p_{111}uvw \end{aligned} \quad (14)$$

where $p_{uvw}$ explains the intensity of pixels corresponding to (u, v, w) coordinates.

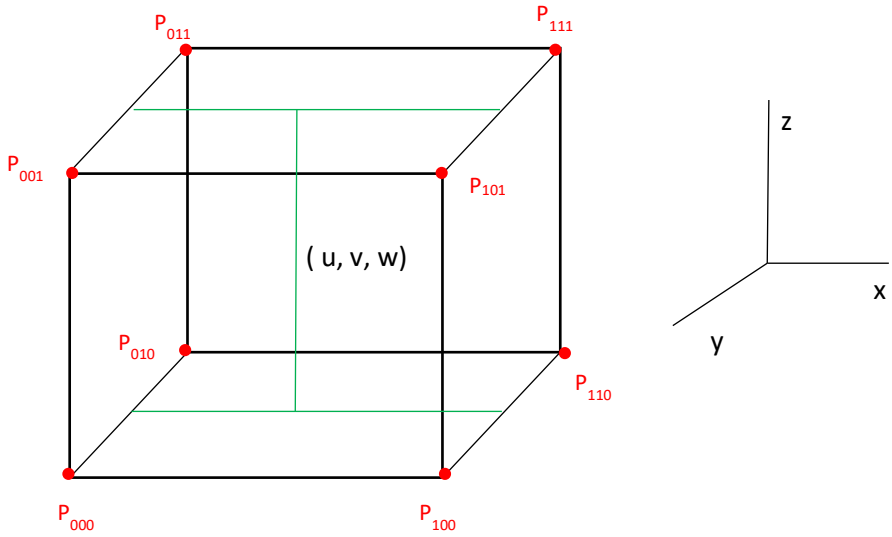


Figure 4-11. The calculation of pixels between two slices based on trilinear interpolation method.

## 4.5. Results and Discussions

According to data from an MRI machine with a set of 44 MRI cortex images provided by Binh Duong General Hospital. The results show that the thresholds with two levels are more significant and efficient to produce the desired image. To reach such procedures using Otsu method, 2D MRI cortex images should be processed for segmentation and enhancement of 2D images in order to reach a 3D brain image construction. In Figure 4-12, Otsu multilevel method is used to segment the image and the region growing method continues to process the segmented image shown as Figure 4-13, (4 and 5). The pixel values for the segmented image is [0,1] which is a binary image. Moreover, Figure 4-12 represents the combination of region growing algorithm and Otsu method with two thresholds from 12 MRI cortex image described in Figure 4-13.

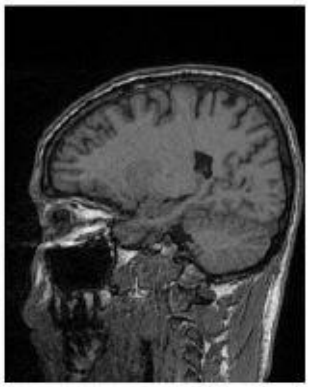

1.Original MRI cortex image

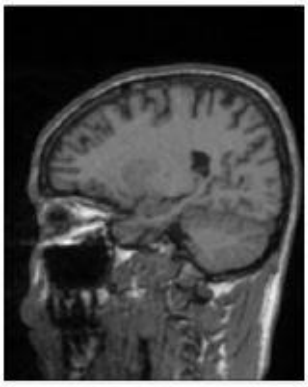

2.Image after average filter

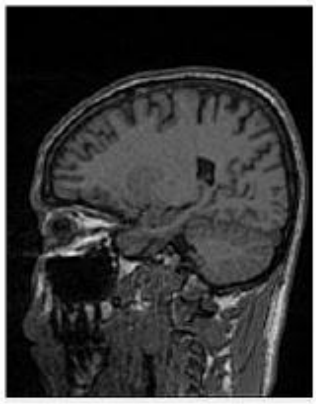

3.Image after unsharp filter

4.Image after enhancement

5.Image after segmentation using the Otsu with two levels

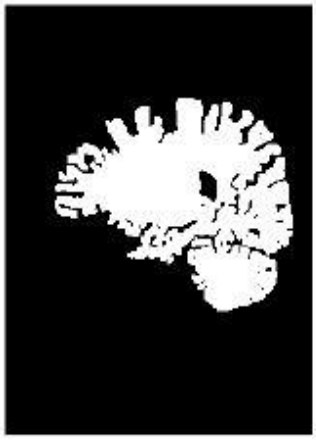

6.Image after segmentation using the region growing using the region growing

Figure 4-12. The pre-processing image representation.

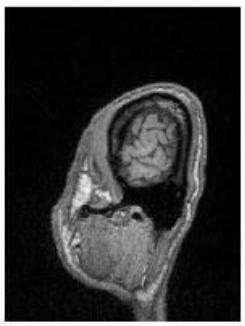

1

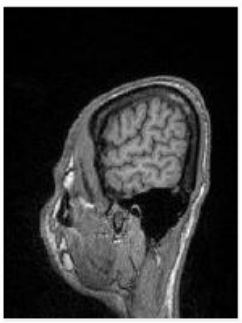

2

3

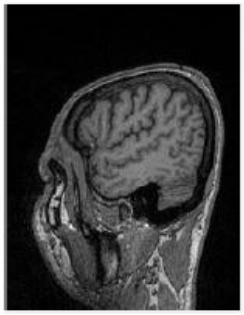

4

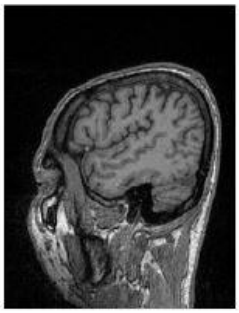

5

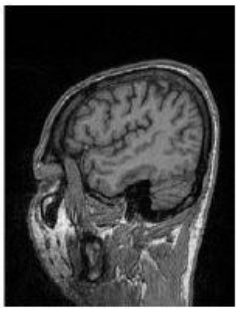

6

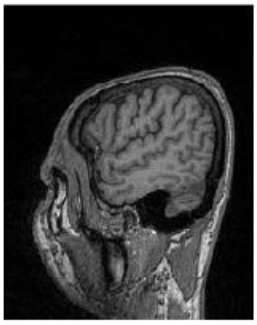

7

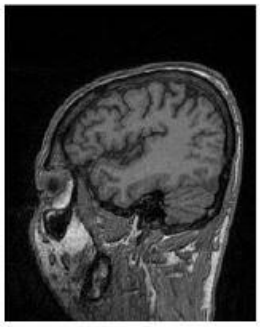

8

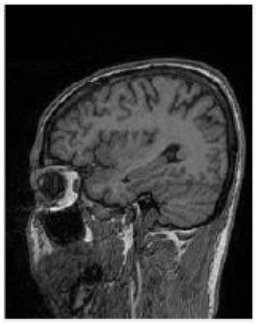

9

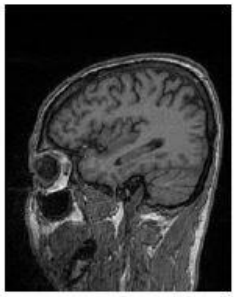

10

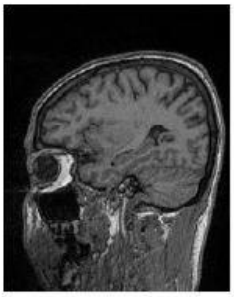

11

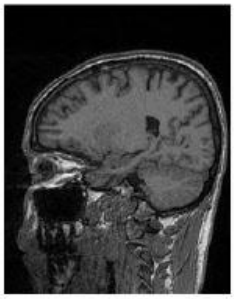

12

Figure 4-13. The morphological cortex images.

The binary images in the whole MRI cortex image sustains the brain part through the segmented brain images. After processing to obtain 3D image, the binary image retains the structure of original image. In addition, the convoluted images in Figure 4-14 are processed between the original images of 12 image slices corresponding to 44 2D MRI cortex images and the segmented image.

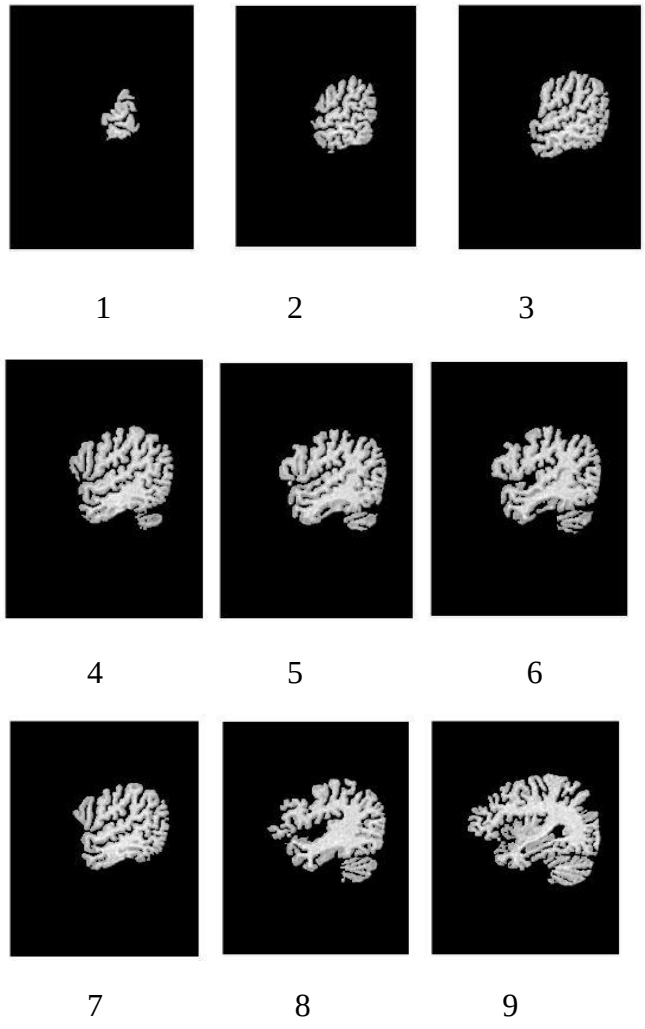

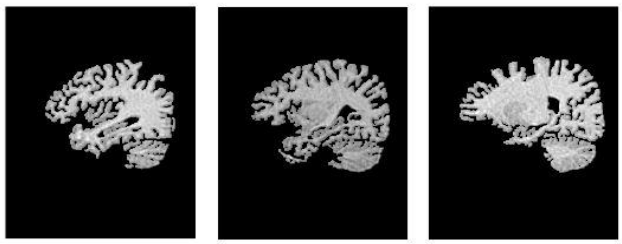

10 11 12

Figure 4-14. Images after convolution .

# CHAPTER 5

# Generative Adversarial Nets (GAN) for Brain Tumor Segmentation

## 5.1. Introduction

According to the statistics provided by the Cancer.net in 2020 (from ASCO), the estimated number of people who will be diagnosed with primary cancerous brain tumor in America is expected to be totally 23,890 adults- 10,300 women and 13,590 men have a high sensitivity in this problem. This year, approximately more than 3500 children are trying to survive brain tumor disease and they also are under the age of 15 and these tumors cover 90% of all CNS tumors (Central Nervous System). However, previous years, the statistics of this disease primarily were estimated to be diagnosed among 80000 children, men and women. The base categories of brain tumors at that time included malignant (cancerous) and benign (noncancerous) tumors [37].

So, it is obvious that brain tumor challenge automatically reflects the life expectancy of human being. Indeed, this segmentation requires high-order smoothing standards and perspectives targeting positive solutions. The current follow-ups and treatment planning can be applied by using 2D measurement to properly identify glioma structures in brain and also non-invasive delineation. Gliomas have been studied as brain tumors from infiltrating tissues and glial cells [38]. Low-grade gliomas (LGG) and High-grade gliomas (HGG) are primary components of those given neoplasms. In case of assessment based on the area of MRI (Magnetic Resonance Imagining) as 2D measurement, this technique (MR) is most efficient sequence to obtain accurate complementary information in evaluation of successful treatment planning in practice. MR allows us to determine the gyromagnetic properties of tissues in the brain and it basically deals with the phenomenon of nuclear resonance. However, there are still many reasons for the problem of gliomas segmentation, because this task cannot be easily segmented in terms of structure of brain tumors and their location. As diagnostics of accurate brain tumor is getting serious issue in treatment planning, automatic or semi-automatic segmentation is expected to be essential instead of arrangement of time-consuming and expensive manual approach. Nowadays both biological and natural image processing is successfully considered as achievement of deep learning of neural network in brain tumor analysis. Compared to other methods, CNN in biological image processing enables us to obtain accurate biomedical problems and to build neural network to show specific diseases such as Alzheimer, lesion and even cancer by scanning specific areas of brain [44]. However, this method no longer

maintains its stability in structuring analysis of brain tumor segmentation, because CNN needs more extensive medical data [39], but indeed it is hard to achieve under desired conditions. The solution for better performance is intensity or geometry transformations as a component of data augmentation techniques which aims reconstructing following original images.

Practically, generalization abilities in performance improvement lead to limitation of better reconstruction of original images, but those images present so realistic image distribution meaning that new images obtained are similar to original ones.

Deep learning generative adversarial networks (GAN) based on generative models and data augmentation is used as a framework to optimize general computer vision tasks. It simply acquires the real outcomes by matching distribution that is generated from entire noise variables. Moreover, GAN creates essential medical diagnostic reliability, potential physician teaching and training, but for some extent, it turns out to be challenging to train these tasks. The reason behind these approaches is that brain MR images with generated potential GAN applications are shown graphically (Figure 5-1) in terms of how realistic pathological images help to better understand misdiagnosis in different diseases by physician training and how data augmentation is better determinant of accurate diagnosis by generating realistic tumor images in random locations.

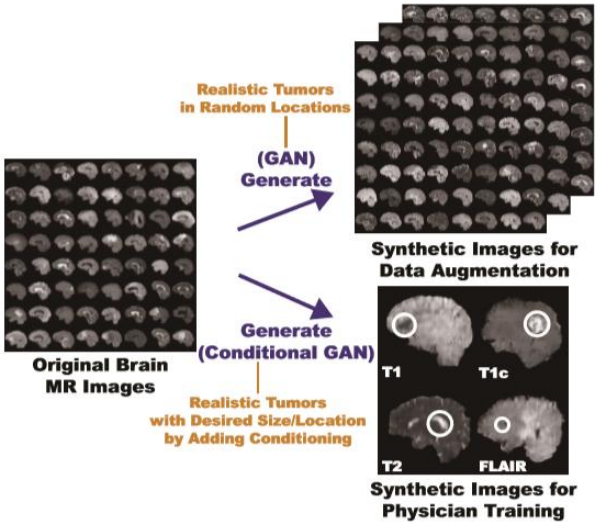


Figure 5-1. The proposed GAN-based synthetic brain MR image generation.

(C. Han *et al.*, "GAN-based synthetic brain MR image generation," *2018 IEEE 15th International Symposium on Biomedical Imaging (ISBI 2018)*, Washington, DC, 2018, pp. 734-738, doi: 10.1109/ISBI.2018.8363678)

## 5.2. Related Works

Anomaly detection, CT images from MR and image super-resolution are areas where mostly GAN is commonly used by researchers in medical image processing. Conditional GANs allow to evaluate desired images by adding conditioning on class images and also labels. The discrepancy appears when it reaches hidden spaces, then learning these robust spaces are getting complicated. Another research based on GANs proposed for fluorescence microscopy (biological synthesis of images) provides details of generated realistic MR images by GANs and data augmentation or physician training.

Our predictions about all label variables depend on how independently they are chosen from each other for any kind of network. The use of conditional random fields (CFR) is a high-order smoothing technique in optimization of output label map with details in it. CRF is a best approach for spatial contiguity considering that post-processing for all label variables in output label maps needs reinforcement of spatial contiguity [79]. Although the application of gaussian kernel frequently defines pairwise potentials [80], the use of potentials is limited for CRF methods. Therefore, instead of focusing CRFs we may propose Generative Adversarial Nets (GAN) framework to detect inconsistencies and correct these higher-orders between segmentation net with maps and group truth segmentation maps [40].

In addition to adversarial training, generating probability maps with five-classification is not stable as much as a segmentation image this is generated as a result of the training of segmentation network. We should consider multi-angle GAN framework according to image-to-image translation and a GAN is fundamental element for generator as it is taken as segmentation network in Luc's method. Actually, the probability maps optimized by Luc's model also combines generative and discriminative models in a direct way. Another model suggests to separate segmentation network and the generator in a practice to generate an image based on feature space where segmentation network and generator share same feature space. Then, we combine the probability maps and generated image that is a single image with five kinds of pixel values (0,0.25,0.5,0.75,1). No matter how the discriminator analyzes the differences between ground truth and generative image, optimization of segmentation results leads to a poor training as it is used in an indirect way. Multi-patch discriminator is most efficient method to train this problem in order to reinforce spatial contiguity instead of proposing GAN segmentation method.

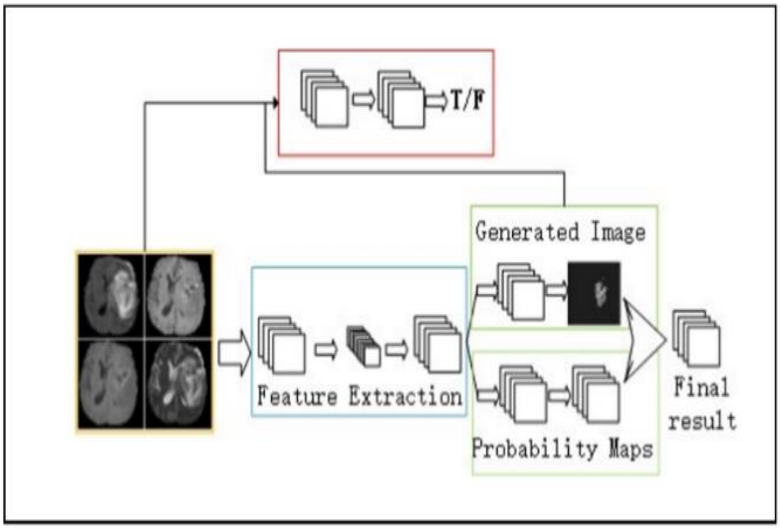


Figure 5-2 . The architecture of framework which include four parts of network: Feature Extraction, Segmentation Part, Generative Part and finally Result Fusion.

(H. Chen, Z. Qin, Y. Ding and T. Lan, "Brain Tumor Segmentation with Generative Adversarial Nets," *2019 2nd International Conference on Artificial Intelligence and Big Data (ICAIBD)*, Chengdu, China, 2019, pp. 301-305, doi: 10.1109/ICAIBD.2019.8836968)

## A. Feature Extraction

Feature extraction of original images begins with classified pixels and generated images. The construction simply demonstrates top-down pathway as similar to generative networks in DCGAN and bottom-up pathway combination in terms of U-net and FPN [41]. Firstly, it might be better to figure out that the top-down pathway is DeconvNet in all layers with a stride of 2. While, the bottom-up pathway as a ConvNet in all layers with conv-stride of 2 targets to extract hierarchical features in which the features are common for four morphological brain images. The goal of top-down pathway is to generate fine-grained features from coarse grained ones by taking input which is the output of bottom-up pathway. In fact, lateral connection combines those features (fine-grained features) obtained following procedures. In fact, there is no need to consider lateral connection in case of 1x1 convolution and to check periodically pyramidal feature as FPN uses.

There are three commonly proposed solutions to determine whether discriminating each image with the class of each pixel and segmentation images generated have same feature representation. The first solution is to choose one pathway for classification and another pathway for generating images and they are called as two parallel pathways.

The second solution is to make 1x1 convolution follow lateral connection as a matter of fact that two mentioned tasks share different DeconvNets, but same ConvNets.

The final solution is to test a hypothesis of knowing same feature space for both five-classification result and generative segmentation image. This hypothesis shows a positive relationship between Generative Part and Segmentation Part in same feature extraction layers optimized by GAN which are basically optimal for classification.

### B. Segmentation Part

This part is providing primary results in a way to analyze optimization method for classification results. The segmentation consists of the probability map which demonstrates the output of segmentation and there are two 1x1 convolution layer as cross-channel parametric polling showing feature map polling mainly used for decreasing feature maps and dimensionality. Since five-classification task shown as brain tumor segmentation and SoftMax classification in the segmentation part are introduced with respect to the function which is basically cross-entroy loss as following:

$$L_{sp} = \sum_i \sum_j \mathbb{I}\{y_{ij} = j\} \log P_{ij} \qquad (15)$$

In this function j and n are labels and number of training data, respectively.

### C. Generative Adversarial Part

Although GAN high-level optimization is key factor to acquire primary results, it has two stages representing generative and discriminative stages where they optimize the primary results not by generating probability maps directly, but indirectly targeting segmentation images.

In this paper, we focus the generator G without second convolution layer that has same structure as segmentation part has accordingly. Additionally, we extract features from Feature Extraction Part in order to generate 240x240 segmentation image. So, patchGAN is a structural technique which can penalize and restrict structure at scale of local image patches. To check whether each patch has real or fake segmentation image, estimated result provided by discriminator D in patchGAN is potentially required. Choosing randomized fixed size patches and their average responses are best fulfillment of patchGAN. For simplicity, we fix output of discriminator and take average of dense responses in a fact that the discriminator consists of different convolutional layers connected with segmentation image and also four-modal images. After several periods of observing training of generator, we analyzed a main difference between ground truth and generative image is not practically conducive and the best

alternative to better solve this problem is to apply multiple-angle patchGAN. The discriminator here is representing multi channels apart from the discriminator with single channel output. Furthermore, the discriminator in multi-angle patchGAN can be explain with an example of people having no only one perspective, but multiple perspectives of looking at object. However, for convenience, we make an argument about difference between ground truth and segmentation images as we mention before and indeed, they both are treated by discriminator. Therefore, we provide the result of the output of D by taking all average responses. The function of generative adversarial loss is as following:

$$L_{GAN}(D;G) = E[\log D(y|x)] + E[\log(1 - D(x))] \quad (16)$$

- Y is shown as the probability distribution of ground truth
- X is shown as the joint probability distribution of four-modal images

Then we apply L1 distance variable to generate better training and image of network:

$$L_{L1}(G) = E[||y - D(x)||] \quad (17)$$

Generative adversarial loss function changes to:

$$L_{GAN} = L_{GAN}(D;G) +|_1 L_{L1}(G) \quad (18)$$

### D. Result Fusion

Even if there are a few differences between generative image and primary result, both results use 1x1 convolutional layer to be jointly significant and final result of segmentation is the output generated. The final function is below shown as sum of following determinants; cross-entropy loss function Lrf is a loss function, similarly Lsp and loss function of generative adversarial part.

$$L = L_{GAN} +|_2 L_{sp} +|_3 L_{rf} \quad (19)$$

## 5.3. Experiments

In this part, we are going to evaluate the deep details of network and segmentation result by using potential network training details and parameters.

### A. Database

BRATS 2020 dataset consists of two sub-datasets including the Testing Set and the Training Set. There are four conceptual modalities in BRATS 2020 in each brain and different abnormal and healthy tissues are described by following each of modalities [42]:

1. T1-weighted (T1) – There is the lowest intensity value in which CSF as an example of Fluids have same outcomes. Gray matter has less intensities compared to white matter shown in Figure 5-3.
2. T2-weighted (T2) – it is another modality which is common MR imaging sequence and part of MR imaging protocols with T1. It has intermediate intensity of grey matter, less intensity of matter and high intensity values of fluids.
3. T1 with gadolinium contrast (T1c) – this MR modality is especially used to highlight breakdowns in inflammation, tumors and even abscesses and vascular structure in these blood-brain barriers is common for this type of modality. The effect of T1 signal increases, while T1 relaxation time decreases.
4. T2 - FLAIR – This image are inverse recovery sequences where they are proposed to obtain bright abnormalities and attenuated dark CSF. The sensitive sequences differentiate an abnormality and CRF during pathology.

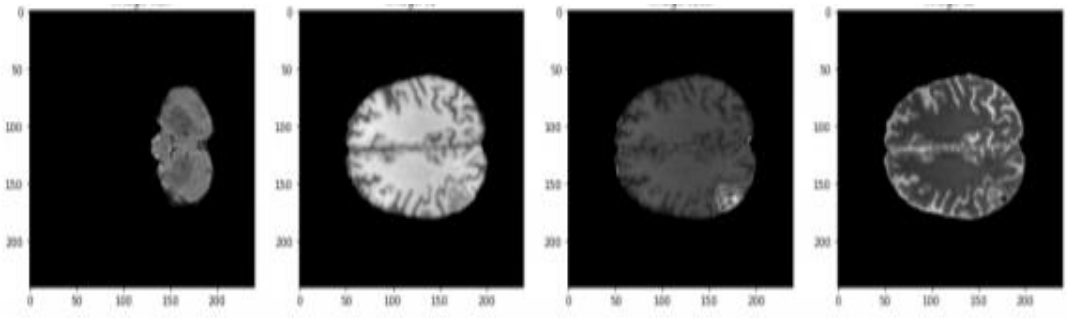

T2-Flair T1-weighted T1- contract gadolinium T2-weighted

Figure 5-3. Four different MR modalities.

(Puch, Santi. (2018). Multimodal brain tumor segmentation in Magnetic Resonance Images with Deep Architectures. 10.13140/RG.2.2.35829.63208)

## B. Experiments Setup

Table 5-1 and Table 5-2 below represent hyper-parameters and batch normalization is a base method applied [86]. Alternatively output and input layers are not included in this analysis for all layers. As it is studied with activation function mainly LRelu,

normal distribution for all variables is N(0,0.002). We experience optimization of network at training time considering $\lambda 2 = \lambda 3 = 1$ and $\lambda 1 = 60$ with 0:9 momentum used as Adam Solver [90] and Minibatch SGD. The epoch is 10, learning rate is 0.0004 and batch size is 5. Randomly selected data follows step by step techniques to train the generator. First is one descent on D and second is twice step on G.

Table 5-1. ARCHITECTURES OF THE GENERATION AND CLASSIFICATION NETWORK.

| layer | Type | Filter size | Stride | #filters |
|---|---|---|---|---|
| 1 | conv | 4*4 | 2*2 | 64 |
| 2-3 | conv | 4*4 | 2*2 | 128 |
| 4-7 | conv | 4*4 | 2*2 | 256 |
| 8 | conv | 4*4 | 2*2 | 512 |
| 9-12 | deconv | 4*4 | 2*2 | 256 |
| 13-14 | deconv | 4*4 | 2*2 | 128 |
| 15 | deconv | 4*4 | 2*2 | 64 |
| 16 | deconv | 4*4 | 2*2 | 32 |
| 17-1 | conv | 4*4 | 1*1 | 64 |
| 17-2 | conv | 4*4 | 1*1 | 64 |
| 18-1 | conv | 4*4 | 1*1 | 5 |
| 18-2 | conv | 4*4 | 1*1 | 1 |
| 19 | conv | 4*4 | 1*1 | 64 |
| 20 | conv | 4*4 | 1*1 | 5 |

Table 5-2. ARCHITECTURES OF THE DISCRIMINATION NETWORK.

| layer | Type | Filter size | Stride | #filters |
|---|---|---|---|---|
| 1 | conv | 3*3 | 2*2 | 64 |
| 2 | conv | 3*3 | 2*2 | 128 |
| 3 | conv | 3*3 | 2*2 | 128 |
| 4 | conv | 3*3 | 2*2 | 128 |

| | | | | |
|---|---|---|---|---|
| 5 | conv | 3*3 | 1*1 | 32 |

### C. Evaluation

In order to train segmentation results and performance, Dice Similarity Coefficient (DSC) is a significant method to be defined and the function is:

$$DSC = 2\times TP/(2\times TP+FP+FN) \quad (20)$$

where TP denotes the number of true positive segmentation, FP is false positive segmentation and FN is false negative segmentation. Tumor core, enhancing tumor and complete tumor with (labels 1+3+4), (labels 4), (labels 1+2+3+4), respectively are basic three tumor sub-compartments. We consider five-classification task in segmentation result where background and normal tissue with number 0, necrosis with 1, edema with 2 and non-enhancing tumor with 3 and 4 are represented at evaluation time.

## 5.4. Results and Discussions

### A) Several methods on HGG

In this section, we practice HGG cases for testing and training in training set. Clearly, 220 HGG cases are selected based on training set in which 30 cases are used for testing and 190 cases are followed by training. Due to high fluctuation in the results, random 30 HGG cases in 220 cases are not mostly recommended as the segmentation among 220 cases highly changes cosidering their difficulties. We commonly use the method of FCN+CRF and OriGan as our framework in the analysis. However, OriGan in practice proposed by Luc is not stable during training procedures and it does not have precise and good results after our observation (Table 5-3). Obviously, Complete tumor is better obtained in our method without GAN, but we get a bad result for segmentation of Tumor core. Ideally, GAN experiences low performance in Enhancing and Tumor core segmentation, but high performance in Complete tumor.

Table 5-3. Several methods on the HGG data

| Method | Complete tumor | Tumor core | Enhancing tumor |
|---|---|---|---|
| FCN+CRF | 0.8306 | 0.7553 | 0.7806 |

| | | | |
|---|---|---|---|
| FCN | 0.800 | 0.801 | 0.770 |
| SegNet+OriGAN | 0.7509 | 0.5876 | 0.5652 |
| SegNet | 0.8744 | 0.7732 | 0.8587 |
| Our method | 0.8838 | 0.7465 | 0.8451 |

### B) Several methods on Testing Set

The result for patchGAN compared to the method without GAN is a complete evaluation method to get an optimal performance shown in Table 5-4. According to testing set BRATS 2020, 274 patient cases are included in training set and 110 patient cases are also added to testing set as our general network evaluation. The comparison among proposed methods is clearly demonstrated in Table 5-4. Havaei focuses patch-based segmentation analysis by using multi-scale CNN. On the other hand, Pereira [43] proposed small filter kernel similarly for patch-based segmentation. Another approach by Kamnitsas was presented for patch-based segmentation by using 3D multi-scale CNN. He also optimized the probability maps named SoftMax by proposing 3D CRF. The results show a better performance for both Havaei and Pereira's method in terms of tumor core and complete tumor. Also the result of our method is better than the methods mentioned and even better than Kamnitsas's method. Compared to 3D segmentation our method is designed for 2D slices segmentation. For this reason, processing a patient brain varies among the methods. For instance, Havaei's method takes about 25s to 3 min and Kamnitsas' method takes 2 min to 3 min, but our method takes 10.8s which has better time efficiency for processing among all methods.

Table 5-4. Several methods on the testing set.

| Method | Complete tumor | Tumor core | Enhancing tumor |
|---|---|---|---|
| Havaei | 0.79 | 0.58 | 0.69 |
| Pereira | 0.78 | 0.65 | 0.75 |
| Kamnitsas | 0.85 | 0.67 | 0.63 |
| Our method | 0.82 | 0.66 | 0.58 |
| SegNet+CREF | 0.81 | 0.64 | 0.60 |

| | | | |
|---|---|---|---|
| SegNet+patchGAN | 0.81 | 0.60 | 0.59 |
| SegNet | 0.79 | 0.63 | 0.51 |

# CHAPTER 6

# Data implementation for GAN-based MR brain images.

## 6.1. Introduction

Generative Adversarial Networks (GAN) presents realistic and promising results in analysis of image generation and deals with training accompanying mode collapse and oscillations that is hard to achieve without a well-defined objective function [92]. Nowadays, GAN is an optimal solution in an image super-resolution for most of medical imaging researchers. It is also more practical to estimate CT images from MR image accordingly. To produce desired images, conditional GANs supports class labels and images by adding conditioning. Moreover, data augmentation and physician training are major approaches focused by GAN-based MR image generation for brain tumor segmentation.

The requirement of few tests is to provide values of hyperparameters before final model evaluation. The parameters include number of filters, fully connect layer size, and filter size [96]. In addition to best values for parameters, dropout rate, or learning rate, optimizer after pre-training the network are more likely to change. The choices of values depend on few tests conducted on training data. According to a 5-fold cross-validation split introduced by Cheng et al., two major issues of random splitting data were resolved using this split for model evaluation. First, the test set does not contain two scans of same patient. Second, the same amount of date is presented in the test data per each class and the results do not illustrate the class imbalance of dataset. Despite the fact that 5-fold validation presents more reliable use of the classification, cross-validation or random train-test split are used in most of the works. Moreover, both introduced and random 5-fold cross-validation are proposed in order to make the results significantly comparable and reasonable.

We will also achieve synthetic brain MR images by using GANs to generate realistic brain images. Whereas Multimodal Brain Tumor Image Segmentation Benchmark (BRATS) produces significantly satisfactory resolution and data for GANs to explore a dataset of multi-sequence MR images. Therefore, T1-weighted (T1), T2-weighted (T2), contrast enhanced T1-weighted (T1c), Fluid Attenuation Inversion Recovery (FLAIR) sequences are resampled to 240 X 240 X 155 image dimension and 1mm X 1mm X mm isotropic resolution. High-Grade Glioma (HGG) and Low-Grade Glioma (LGG) support the sequences among different sectional planes to generate the whole

brain anatomy. This procedure allows us to show visual consistency among various brain lobes. In Figure 6-1, real MR images specifies training of the GANs by using resized sagittal multi-sequence MRI scans with HGG for patients.

In this Chapter, we compare two GAN-based approaches to avoid mode collapse through well-suited GAN between Deep Convolutional GAN (DCGAN) and Wasserstein GAN (WGAN) for realistic MR image generation with high resolution. In the second part, we will also study GAN pre-training based MRI images through statistically testing both random and introduced splits based classification after GAN-pre training. These tests will explain highest accuracy of different types of brain tumors in order to reach best tumor segmentation results.

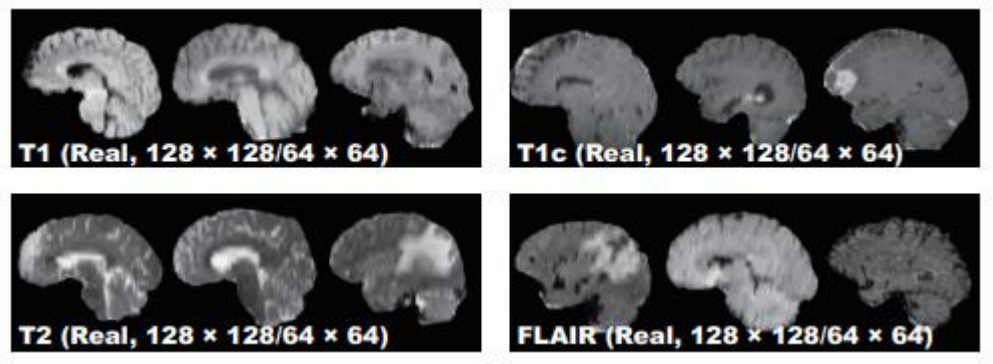


Figure 6-1. Real MR images for training the GANs

## 6.2. Pre-processing approach

We practiced #80 to #149 slices to eliminate final slices among all 240 slices in order to obtain sufficient data as a part of the training. 64 x 64 (stable training for DCGAN architecture results) and 128 x 128 (a high-resolution) are the sizes of images for effective GAN training from 240 x 155 [46]. In Figure 6-1, GAN training based real MR images with patients of HGG shows 15,400 images for each sequence in terms of 220 patients x 70 slices, but 61,600 in total.

## 6.3. GAN-based MR Image Generation

Six types of images are generated by WGAN and DCGAN;

T1 sequence with 128 x 128 size from the real T1

T2 sequence with 128 x 128 size from the real T2

T1c sequence with 128 x 128 size from the real T1c

FLAIR sequence with 128 x 128 size from the real FLAIR

Concat sequence with 128 x 128 size from all the MRI sequences (the real T1, T2, T1c, FLAIR)

Concat sequence with 64 x 64 size from all the MRI sequences (the real T1, T2, T1c, FLAIR)

Concat sequence contains the features of all four sequences that refers to alternative data augmentation. In addition to Concant sequence, 64 x 64 images compare the performance of generation by considering image size.

**WGAN:** It achieves stable learning through replacing less mode collapse to the Earth Mover (EM) distance and an alternative to traditional GAN training. In equation 21, ∏ (pg, pr) shows respective marginals pg and pr for a set of joint distributions p, but p is a determinant of transporting one distribution to another one in terms of amount of mass.

$$W(p_g, p_r) = \inf_{p \in \Pi(p_g, p_r)} E_{(x,x') \sim p} \|x - x'\|, \qquad (21)$$

**Implementation details of WGAN:** We implement learning rate of 5.0 x 10^(-5) with Root Mean Square Propagation (RMSprop) optimizer, as well as a batch size of 64.

**DCGAN:** This generative model achieves unsupervised learning through convolutional architecture being as a standard GAN. It uses a combination of batch-normalization and non-linearity as a part of up-convolutions. Consider pdata is generating distribution and data space on input noise variable for generator G (z, θg) is pz (z). In this term, G with parameters θg is a neural network. In addition, D (x, θd) with parameters θd uses synthetic data and real data. X comes from the real data and D (x, θd) is a neural network. D is a discriminator that maximizes samples from G and probability of classifying training examples. However, G is a generator that minimizes the likelihood. In equation 22, value function V (G, D) is formulated for two-player game as a minimax. This formulation is the minimization of Jensen-Shannon (JS) that is divergent between distribution pg and distribution pdata due to derivation of pz and G.

$$\min_G \max_D V(D,G) = E_{x\sim p_{data}(x)}[\log D(x)] + E_{z\sim p_z(z)}[\log(1 - D(G(z)))] \quad (22)$$

**Implementation details of DCGAN:** We implement learning rate of 2.0 x 10^(-4) with Adam optimizer, as well as a batch size of 64. A half channel size for DCGAN training, 4 X 4 sized filters, discriminator ELU and DCGAN architecture in the generator with no tanh are used to better analyze the satisfactory results.

### 6.4. GAN generated MR Images.

This part shows generated synthetic brain MR images obtained by WGAN and DCGAN. The training during classification of random selection of 50 real/50 synthetic MR images took 2 hours to define 128 x 128 and 64 x 64 sequences separately. The results show how to identify the quantitative evaluation of the realism and instances of synthetic images. Moreover, the sequences are demonstrated on learning realistic features that include Nvidia GeForce GTX 980 GPU.

**WGAN:** Synthetic MR images proposed by WGAN in Figure 6-2 shows successful appearance of the tumors and the sequence-specific texture in realistic original MR brain images. Whereas unexpected intensity patterns suggest unrealistic artifacts from 128 x 128 Concat images compared to 64 x 64 Concat images which are mostly experienced around the boundaries of the brain.

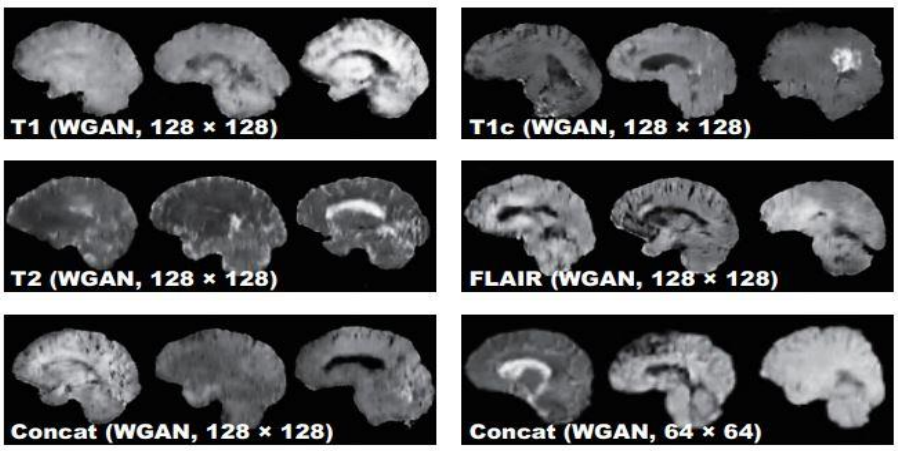


Figure 6-2. Synthetic MR images based on WGAN.

**DCGAN:** Synthetic MR images proposed by DCGAN in Figure 6-3 shows unstable value function and generates hyper-intense images similar to T1 for mode collapse of

64 x 64 Concat images. In this generative model, all four sequences are used for combination of patterns and appearances via Concat images.

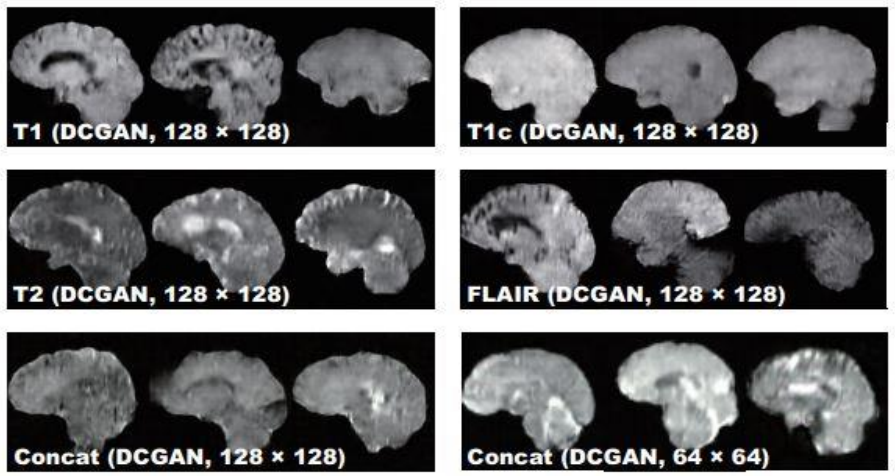


Figure 6-3. Synthetic MR images based on DCGAN.

Table 6-1. The physician classified real and synthetic images accordingly according to Visual Turing Test (VTT). 50% in the test indicates excellent performance in accuracy as it is a chance = 50%.

| | **Accuracy (%)** | **Real Selected as Real** | **Real as Synthetic** | **Synthetic as Real** | **Synthetic as Synthetic** |
|---|---|---|---|---|---|
| T1 (WGAN, 128x128) | 64 | 20 | 30 | 6 | 44 |
| T1c (WGAN, 128x128) | 55 | 13 | 37 | 8 | 42 |
| T2 (WGAN, 128x128) | 58 | 19 | 31 | 11 | 39 |
| FLAIR (WGAN, 128x128) | 62 | 16 | 34 | 4 | 46 |
| Concat (WGAN, 128x128) | 66 | 31 | 19 | 15 | 35 |
| Concat (WGAN, 128x128) | 53 | 18 | 32 | 15 | 35 |
| T1 (DCGAN, 128x128) | 70 | 26 | 24 | 6 | 44 |
| T1c (DCGAN, 128x128) | 71 | 24 | 26 | 3 | 47 |

| | | | | | |
|---|---|---|---|---|---|
| T2 (DCGAN, 128x128) | 64 | 22 | 28 | 8 | 42 |
| FLAIR (DCGAN, 128x128) | 54 | 12 | 38 | 8 | 42 |
| Concat (DCGAN, 128x128) | 77 | 34 | 16 | 7 | 43 |
| Concat (DCGAN, 128x128) | 54 | 13 | 37 | 9 | 41 |

## 6.5. GAN pre-training based on MRI images

Table 6-1 and 6-2 show different learning rates and different optimizers based on these tests. The dropout rate with 0.5 and learning rate with 0.001 are assigned to the optimizer Adam algorithm as described in Table 6-2 and 6-1, respectively. Table 6-3 demonstrates the results on introduced split based on classification after GAN-pre training while Table 6-4 introduces the results on random split based classification after GAN-pre training. Furthermore, the results without GAN pre-training is illustrated in Table 6-5. In Figure 6-4, it is obvious that GAN pre-training proposes model accuracy on learning pace. An increase in epoch leads to an increase in accuracy rate over time depending on the model with or without GAN. In Table 6-6, summary of results on the main dataset suggests various methods, approximate number of images used in those methods, evaluation methods, manual segmentation, and accuracy rates according to reported outcomes on given methods. In fact, the method proposed by Phaye et al., and GAN + ConvNet (random split) represent the highest accuracy rates among other methods with 95.03% and 95.6%, respectively. The comparisons of methods in Table 6-6 reveals that Convolutional Neural Network (CNN) without manual segmentation shows overall better performance with high accuracy rate. Whereas CNN pre-training as a GAN discriminator is highly applicable in deep learning depending on limited number of data.

### 6.5.1. Tables

Table 6-1: The difference between various optimizers and learning rates.

| Optimizer | Learning rate | | | | |
|---|---|---|---|---|---|
| | 1 | 0.1 | 0.01 | 0.001 | 0.0001 |
| SGD [47] | 30.83 | 47.15 | 70.80 | 75.53 | 69.00 |
| RMSprop [47] | 30.83 | 30.83 | 47.15 | 93.64 | 89.56 |
| Adam [48] | 47.15 | 47.15 | 47.15 | 95.27 | 91.35 |
| Adadelta [49] | 94.45 | 90.70 | 71.45 | 48.12 | 39.15 |
| Adagrad [50] | 47.15 | 47.15 | 92.82 | 87.28 | 68.52 |

Table 6-2: The difference between different dropout rates.

| Dropout rate | 0.1 | 0.3 | 0.5 | 0.7 | 0.9 |
|---|---|---|---|---|---|
| Accuracy | 94.78 | 95.27 | 95.27 | 94.12 | 47.15 |

Table 6-3: The results for GAN pre-train on introduced split.

| Class | Accuracy | Sensitivity | Specificity | Precision | F1-score |
|---|---|---|---|---|---|
| Glioma | 94.95 | 94.92 | 94.95 | 94.16 | 94.53 |
| Meningioma | 93.71 | 84.82 | 96.41 | 87.64 | 86.12 |
| Pituitary tumor | 97.35 | 96.29 | 97.80 | 95.05 | 95.63 |
| Total | 93.01 | 92.01 | 96.39 | 92.28 | 92.10 |

Table 6-4: The results for GAN pre-train on random split.

| Class | Accuracy | Sensitivity | Specificity | Precision | F1-score |
|---|---|---|---|---|---|
| Glioma | 96.60 | 96.83 | 96.38 | 95.89 | 96.35 |
| Meningioma | 96.01 | 89.98 | 97.79 | 92.43 | 91.19 |
| Pituitary tumor | 98.60 | 97.93 | 98.89 | 97.54 | 97.73 |
| Total | 95.60 | 94.91 | 97.69 | 95.29 | 95.10 |

Table 6-5: The results without GAN pre-train on introduced split.

| Class | Accuracy | Sensitivity | Specificity | Precision | F1-score |
|---|---|---|---|---|---|
| Glioma | 93.84 | 94.96 | 92.77 | 91.93 | 93.42 |
| Meningioma | 92.82 | 79.86 | 96.76 | 87.96 | 83.63 |
| Pituitary tumor | 96.73 | 95.67 | 97.21 | 93.61 | 94.58 |
| Total | 91.70 | 90.16 | 95.58 | 91.17 | 90.54 |

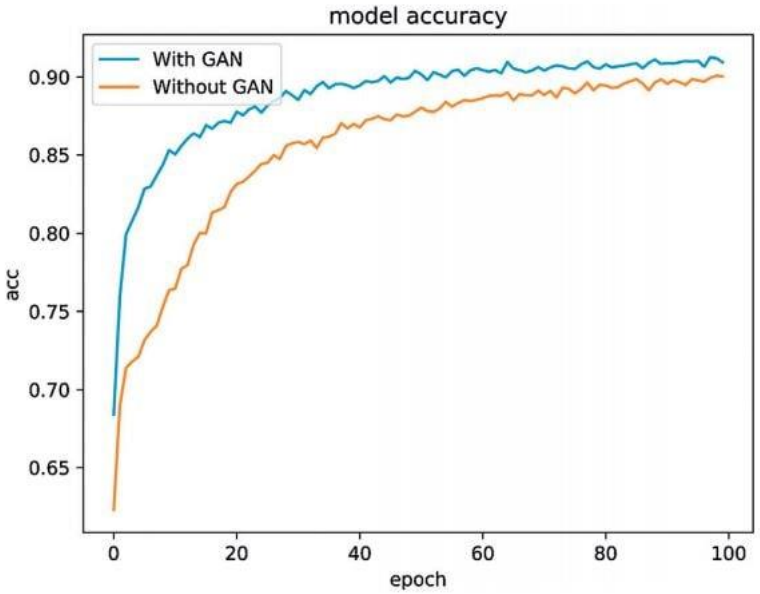


Figure 6-4. Model accuracy of GAN pre-training effect on learning pace.

Table 6-6. Comparison of our method with reported results on the main dataset.

| **Method** | **Number of images used** | **Best accuracy** | **Manual segmentation** | **Evaluation method** |
|---|---|---|---|---|
| Paul et al. ConvNet, 64 × 64 | 989 (axial only) | 84.52 | No | 5-Fold |
| Paul et al. ConvNet, 256 × 256 | 989 (axial only) | 90.26 | No | 5-Fold |
| Phaye et al. [51] Diverse CapsNet | 3064 | 95.03 | Not mentioned | 10-Fold |
| Tahir et al. [52] SVM + Preprocessing | 3064 | 86 | No | 10-Fold |
| Afshar et al. CapsNet | 3064 | 86.56 using segmentation 72.13 on raw images | Both | Not mentioned |
| Ismael and Abdel-Qader [53] Statistical features | 3064 | 91.9 | Yes | Train-validation |
| Afshar et al. [54] CapsNet | 3064 | 90.89 | Only bounding box | Not mentioned |

| | | | | |
|---|---|---|---|---|
| Pashaei et al. [55] KE-CNN | 3064 | 93.68 | Not mentioned | Train-validation |
| Anaraki et al. [56] GA+ CNN | 989 (axial only) | 94.2 | No | Train-validation |
| Abiwinanda et al. [57] Different ConvNets | 2100 (700 from each tumor type) | 84.19 | No | Train-validation |
| Zhou et al. [58] LSTM +Autoencoder | 989 (axial only) | 92.13 | No | Train-validation test |
| Cheng et al. Bag of words | 3064 | 91.28 | Yes | Introduced split |
| Ours, GAN + ConvNet (introduced split) | 3064 | 93.01 | No | Introduced split |
| Ours, GAN + ConvNet (random split) | 3064 | 95.6 | No | 5-Fold |

## 6.6. Results and Discussions

### 6.6.1. Visual Turing Test (VTT)

Even though the physician felt odd from artificial sequence and classified real and synthetic images provided by Visual Turing Test (VTT), Concat images compared to T1, T2, T1c and FLAIR images are evaluated uniformly. The images were more challenging due to less detailed appearances in lower resolution and 64 X 64 Concat images by DCGAN that was highly hyper intense. However, WGAN generates good generalization for multi-sequence brain MR images to clinical applications. DCGAN does not provide suitable results due to mode collapse and inferior realism. WGAN only fails in FLAIR (128 x 128) as it has 62% accuracy rate compared to 54% accuracy rate for DCGAN FLAIR (128 x 128).

### 6.6.2. GAN pre-training results

Pre-training and fine-tuning are major two phases of learning algorithm in our method. Pre-training method solves size problem of low dataset while and it can use any MRI dataset. Based on our results, the overall performance was optimistic and prevailing in terms of proposed pre-training method. A discriminator in GAN was considered as the pre-training for deep network. Glioma tumor (1426 images), Meningioma tumor (708 images), and Pituitary (920 images) are three brain tumor types that are components of final classification task as T1 type in MRI scans. 93.01% accuracy rate for the

introduced split and 95.6% accuracy rate for a random split were achieved compared to previous methods and works proposed by researchers. According to generative adversarial nets (GAN) limitations, 64 X 64 was the network input size. This process is not using other architectures except GAN as the discriminator due to larger input size. On the other hand, a few works illustrated effective results in creating 256 X 256 images [59]. Such methods can be analyzed through deep CNNs such as ResNet-152 or VGG-16.

# CHAPTER 7

## 7.1. Conclusion

The preliminary results show unsuitable implementation of DCGAN for realistic multi-sequence brain images in terms of intensity due to mode collapse and inferior realism. In contract, WGAN has an ability to better generalize and generate 128 X 128 realistic multi-sequence MR images for brain segmentation by the fact that an expert physician could not distinguish the images from real accurately.

The study suggests that more objective computational GAN-based evaluation methods such as Classifier Two-Sample Tests (C2ST) [60] needs to be followed for assessing two samples that are drawn from same distribution. In future, transverse and coronal images will be common demanding applications to analyze more detailed segmentation processes. It is clear that images that are more realistic do not always mean better data augmentation meaning that we generate Concat images and high-resolution images in a way to find suitable image sequences. According to physician training, adding conditioning to generate desired realistic tumors requires the latent space of GANs.

To sum up, we examined the effect of end-to-end network architecture for brain tumor segmentation proposed by GAN. The end-to-end framework speeds up the image processing and solve the issue for repeated calculations. Although the generator and the segmentation net present same feature extraction part, they are different in our method by the fact that the generator is not segmentation net. Comparing with our method analyzed, the generator and generative adversarial training generate and optimize SoftMax probability maps, respectively and these traditional segmentation methods by GAN are difficult in the network to be trained. Furthermore, the generator makes single segmentation images generated and those images achieve final segmentation result after joining SoftMax probability maps. The concept of multiangle patchGAN is introduced to raise the issue for discriminator where the problem can be detected between the generative image and the ground truth. Finally, we practiced CNN-based segmentation models and evaluated the network in BRATS 2020. As the results vary across proposed methods, we achieved 10.8s to process a single patient brain. Unlike the result with average DSC of 0.82, 25s to 3 min required to achieve the processing same patient brain. Overall, our analysis for GAN-based MR images uniformly highlights suitable image resolutions and realistic tumors by medical applications. Future studies on GAN-based realistic MR image applications for brain

tumor will support prognostic and diagnostic medical contributions to reach satisfactory results.

## Glossary

| | |
|---|---|
| **GAN** | Generative adversarial network |
| **DA** | Diagnostic analytics |
| **MRI** | Magnetic Resonance Imaging |
| **CNN** | Convolutional neural networks |
| **FCM** | Fuzzy C-means |
| **MRF** | Markov Random Fields |
| **SVM** | Support Vector Machines |
| **MR** | Magnetic Resonance |
| **FKSRG** | Fuzzy Knowledge-based Seeded Region Growing |
| **FGFCM** | Fast Generalized FCM |
| **BCFCM** | Bias-Corrected FCM |
| **GAs** | Genetic Algorithm |
| **PSO** | Particle Swarm Optimization |
| **EM** | Expectation Maximization |
| **CRF** | Conditional Random Fields |
| **NC** | Necrotic Core |
| **E** | Edema |
| **AC** | Active Cells |
| **SHE** | Spatial accuracy-weighted Hidden Markov random field and Expectation maximization |
| **HMRF** | Hidden MRF |
| **GVF** | Gradient Vector Flow |
| **GDM** | Geometric Deformable Models |
| **CFF** | Charged Fluid Framework |
| **CFM** | Charged Fluid Model |
| **DSC** | Dice Similarity Coefficient |
| **MI** | Mutual Information |
| **DSC** | Dice Similarity Coefficient |
| **ROC** | Receiver Operating Characteristic curve |
| **CT** | Computed Tomography |
| **PET** | Position Emission Tomography |